The 15th Symposium on Polar Science

3－5 December 2024

National Institute of Polar Research

Research Organization of Information and Systems

Session OS

Space and Upper Atmospheric Sciences

Abstracts

Conveners: Masaki Okada, and Yoshimasa Tanaka (NIPR)

OSo1

Exploring Advances in Space Weather Research: AASWO's Contribution to Antarctic Observations

Dr. Adriana Maria Gulisano[1,2,3] , Dr. Sergio Dasso[2,3,4] , Eng. Lucas Tomás Rubinstein [2,5] , Tech. Omar Areso[2] , Eng. Matías Hernán Pereira[2] , Lic. Noelia Ayelén Santos[4] , Lic. Christian Gutiérrez[2,4]

[1] *Instituto Antártico Argentino/Dirección Nacional del Antártico, Buenos Aires, Argentina.*
[2]*CONICET, Universidad de Buenos Aires, Instituto de Astronomía y Física del Espacio, grupo LAMP, Buenos Aires, Argentina.*
[3]*Universidad de Buenos Aires, Facultad de Ciencias Exactas y Naturales, Departamento de Física, Buenos Aires, Argentina.*
[4]*Universidad de Buenos Aires, Facultad de Ciencias Exactas y Naturales, Departamento de Ciencias de la Atmósfera y los Océanos, grupo LAMP, Buenos Aires, Argentina.*
[5]*Universidad de Buenos Aires, Facultad de Ingeniería, Departamento de Electrónica, Laboratorio de Acústica y Electroacústica, Ciudad Autónoma de Buenos Aires, Argentina*

The Argentine Antarctic Space Weather Observatory (AASWO) is leading efforts to deepen the understanding of space weather phenomena. Since its launch in February 2019, AASWO has established a cutting-edge space weather laboratory at the Argentine Antarctic Marambio Station. This facility, managed by the Argentine Space Weather Laboratory (LAMP, http://www.iafe.uba.ar/u/lamp/spaceweather_landing_page.html) is equipped with advanced instruments including a cosmic ray detector, magnetometers, and a meteorological station. Designed to endure the harsh Antarctic conditions, the laboratory features robust construction capable of withstanding extreme cold and high winds. It includes advanced systems such as redundant power sources with gel batteries, materials suited for the Antarctic environment, and precise GPS time stamping to ensure the accuracy of data. The facility's real-time data collection enables immediate transmission of information to LAMP servers in Buenos Aires, facilitating the delivery of space weather products through the LAMP web portal (http://spaceweather.at.fcen.uba.ar/2/index.html).
In its ongoing mission, AASWO expanded its network of space weather laboratories. A new laboratory was constructed at the San Martín station within the Antarctic Circle, marking the addition of a second node to the network. This expansion has taken place during the Austral Summer Campaign 2024. By strategically positioning these laboratories across Antarctica, AASWO aims to address significant gaps in space weather monitoring at high latitudes. Additionally, discussions are in progress regarding the integration of Cherenkov detector data into the Neutron Monitor Database (NMDB) following thorough testing and calibration. This integration is anticipated to greatly benefit the scientific community by providing broader access to vital data and fostering greater collaboration in research.

References

Noelia Ayelén Santos, Sergio Dasso, Adriana María Gulisano,Omar Areso, Matías Pereira, Hernán Asorey y Lucas Rubinstein. First measurements of periodicities and anisotropies of cosmic ray flux observed with a water-Cherenkov detector at the Marambio Antarctic base. Advances in Space Research (2022). https://doi.org/10.1016/j.asr.2022.11.041.

Gulisano, A. M. ; Dasso, S. ; Areso, O. ; Pereira, M. ; Santos, N. A. ; López, V. ; Lanabere, V. ;Ochoa, H. State of the art and challenges of the Argentine space weather laboratory (LAMP) in the Antarctic Peninsula. Boletín de la Asociación Argentina de Astronomía, vol. 62, p.280-285. July 2021

Kelvin-Helmholtz Instabilities and Tube and Knot Dynamics: The Role of Shear Turbulence in Atmospheric Mixing

Tyler Mixa[1], David Fritts[1], Thomas Lund[1], Dominique Pautet[2] and Abhiram Doddi[3]
[1]*GATS-inc., Boulder, Colorado, USA*
[2]*Utah State University, Logan, Utah, USA*
[3]*University of Colorado Boulder, Boulder, Colorado, USA*

Kelvin-Helmholtz instabilities (KHI) accompany strong shear layers throughout the atmosphere where the Richardson number decreases below 0.25. KHI arise from sheet and layer structures when the background wind shear is locally enhanced by gravity wave (GW) propagation and breaking. The mechanism of KHI breakdown can determine how GW energy transport and momentum deposition contribute to atmospheric mixing. Because KHI occur at very small scales, general circulation models (GCMs) do not include KHI and only account for mixing through GW parameterizations. GCMs underestimate mixing in the mesosphere and lower thermosphere (MLT) by up to 50% (Liu et al., 2021), suggesting that KHI and other small-scale dynamics must be contributing to mixing. Here, we present two recent studies that show how KHI can produce more mixing in the atmosphere through tube and knot (T&K) dynamics. KHI with T&K are shown to increase mixing from KHI events by 10-30% in the MLT (Mixa et al., 2023) and 60% in the stratosphere (Mixa et al., 2024). We also present observations of KHI-GW interactions in the MLT that reveal how GWs amplify KHI and produce T&K dynamics. These results motivate us to investigate mixing from KHI in the troposphere. We conclude by showing how data from the 2023-2024 GODSILA field campaign will be used to study KHI at Syowa Station.

References

Liu, H. L., Effective vertical diffusion by atmospheric gravity waves, Geophysical Research Letters, 48(1), e2020GL091474, 2021.

Mixa, T. S., Fritts, D. C., and Lund, T. S., KHI tube and knot dynamics in a weakly unstable stratospheric mixing event, Journal of Geophysical Research: Atmospheres (submitted), 2024.

Mixa, T. S., Lund, T. S., and Fritts, D. C., Modeling Kelvin Helmholtz instability tube and knot dynamics and their impact on mixing in the lower thermosphere, Journal of Geophysical Research: Atmospheres, 128, e2023JD039249, 2023.

Coordinated Radar and HYFLITS Balloon Observations of Atmospheric Turbulence at Syowa Station

Abhiram Doddi[1], Hubert Luce[2], Tyler Mixa[3], Dale Lawrence[1], and Yoshihiro Tomikawa[4]

[1]*Smead Aerospace Engineering, University of Colorado, Boulder, USA*
[2]*RISH, Kyoto University, Japan*
[3]*Global Atmospheric Technologies and Sciences, Boulder, USA*
[4]*National Institute of Polar Research, Japan*

Atmospheric gravity wave (GW) sources, wave breaking dynamics, multiscale Kelvin-Helmholtz instability (KHI) dynamics, and the ensuing turbulent energetics and mixing remain uncharacterized in remote regions along the eastern Antarctic coast. The sources driving multi-scale turbulent atmospheric processes are under-resolved in the state-of-the-art regional weather prediction and global climate models and their influences are misrepresented (Geller et al. [2013]). Comprehensive measurements quantifying the GW momentum fluxes and the turbulence kinetic energy dissipation rate are needed to realistically constrain the GW and KHI sources in sub-grid scale parameterization schemes where observation data is sparse/unavailable (Xue et al. [2012], McLandress et al. [2012]).

The GODSILA field campaign (Guided Observations of Dynamic Shear Instability Layers over Antarctica) was conceived to employ high-resolution in situ turbulence instruments to measure multiscale atmospheric gravity wave (GW) sources and Kelvin-Helmholtz instabilities (KHI) emerging on a wide range of scales and background environments in the coastal Antarctic region around Syowa Station. The figure shows a schematic sketch of the GODSILA field operations at Syowa Station during the Japanese Antarctic Research Expedition (JARE65). The PANSY radar and in situ balloon measurements in conjunction with twice daily Meisei radiosonde measurements quantified the contributions of GW and KHI phenomena to the momentum and turbulence energy budgets in the tropo-stratosphere during Austral summer of 2023-24.

The atmospheric conditions during the 44 days of the GODSILA campaign were characterized by weak Northeast winds, < 20 [m/s]. The weak winds had the advantage of limiting the horizontal drift of the HYFLITS balloons to a maximum of $50 - 150$ [km] from the radar site. The predominant surface winds from the Northeast exhibited steep directional shear between $4 - 5$ [km] and aligned with the upper-level tropospheric jet stream typically prevalent in the eastward - south eastward direction that strengthens up to 40 [m/s] between $5 - 12$ [km].

The preliminary comparisons between the 40 HYFLITS in situ observations dataset and radar measurements show that atmospheric conditions such as horizontal wind, wind shear, and Richardson number of gradient were similar during the ascent and descent of the HYFLITS sondes. This observation is important for future intercomparisons to verify the hypothesis of horizontal homogeneity of the background conditions. Preliminary analysis of the HYFLITS balloon data revealed the presence of frequent localized atmospheric gravity waves. However, a comparison of the HYFLITS and PANSY radar echoes that assessed the turbulence parameters showed that atmospheric conditions were not favorable to intense localized turbulence events. Multiple HYFLITS balloons were launched during each of the three blizzards during the GODSILA campaign. The blizzards were accompanied by strong, yet short-lived, orographic wave activity in conjunction with strong shear regions between $4 - 6$ [km], which produced moderately strong turbulent layers. However, a few sporadic turbulent events related to shear instabilities were identified above 15 [km] altitude, just below the tropopause, and in the troposphere after the 23 December storm according to radar echo properties. The radar observed the most prominent turbulent events below stratiform cloud tops at $4 - 5$ [km] altitude, possibly due to convective instabilities generated by radiative cooling. A directional shear approaching 5 [km] on ascent as the wind rotates from the south to the east, and a weak tropopause layer shown in the temperature profile was a commonly observed feature in most HYFLITS flights.

In this presentation, the GODSILA field campaign data sets will be outlined. The use of high-resolution turbulence data sets acquired from the HYFLITS balloon-borne platform will be discussed in detail. The use of in situ and PANSY radar data collected during the GODSILA field campaign in initializing constraining DNS datasets will be briefly discussed.

References

M. A. Geller, M. J. Alexander, P. T. Love, J. Bacmeister, M. Ern, A. Hertzog, E. Manzini, P. Preusse, K. Sato, A. A. Scaife, and T. Zhou. A Comparison between Gravity Wave Momentum Fluxes in Observations and Climate Models. *Journal of Climate*, 26(17):6383–6405, 2013. doi: 10.1175/JCLI-D-12-00545.1. URL `https://journals.ametsoc.org/view/journals/clim/26/17/jcli-d-12-00545.1.xml`.

C. McLandress, T. G. Shepherd, S. Polavarapu, and S. R. Beagley. Is Missing Orographic Gravity Wave Drag near 60°S the Cause of the Stratospheric Zonal Wind Biases in Chemistry–Climate Models? *Journal of the Atmospheric Sciences*, 69(3):802–818, 2012. doi: 10.1175/JAS-D-11-0159.1. URL `https://journals.ametsoc.org/view/journals/atsc/69/3/jas-d-11-0159.1.xml`.

X.-H. Xue, H.-L. Liu, and X.-K. Dou. Parameterization of the inertial gravity waves and generation of the quasi-biennial oscillation. *Journal of Geophysical Research: Atmospheres*, 117(D6), mar 2012. ISSN 0148-0227. doi: https://doi.org/10.1029/2011JD016778. URL `https://doi.org/10.1029/2011JD016778`.

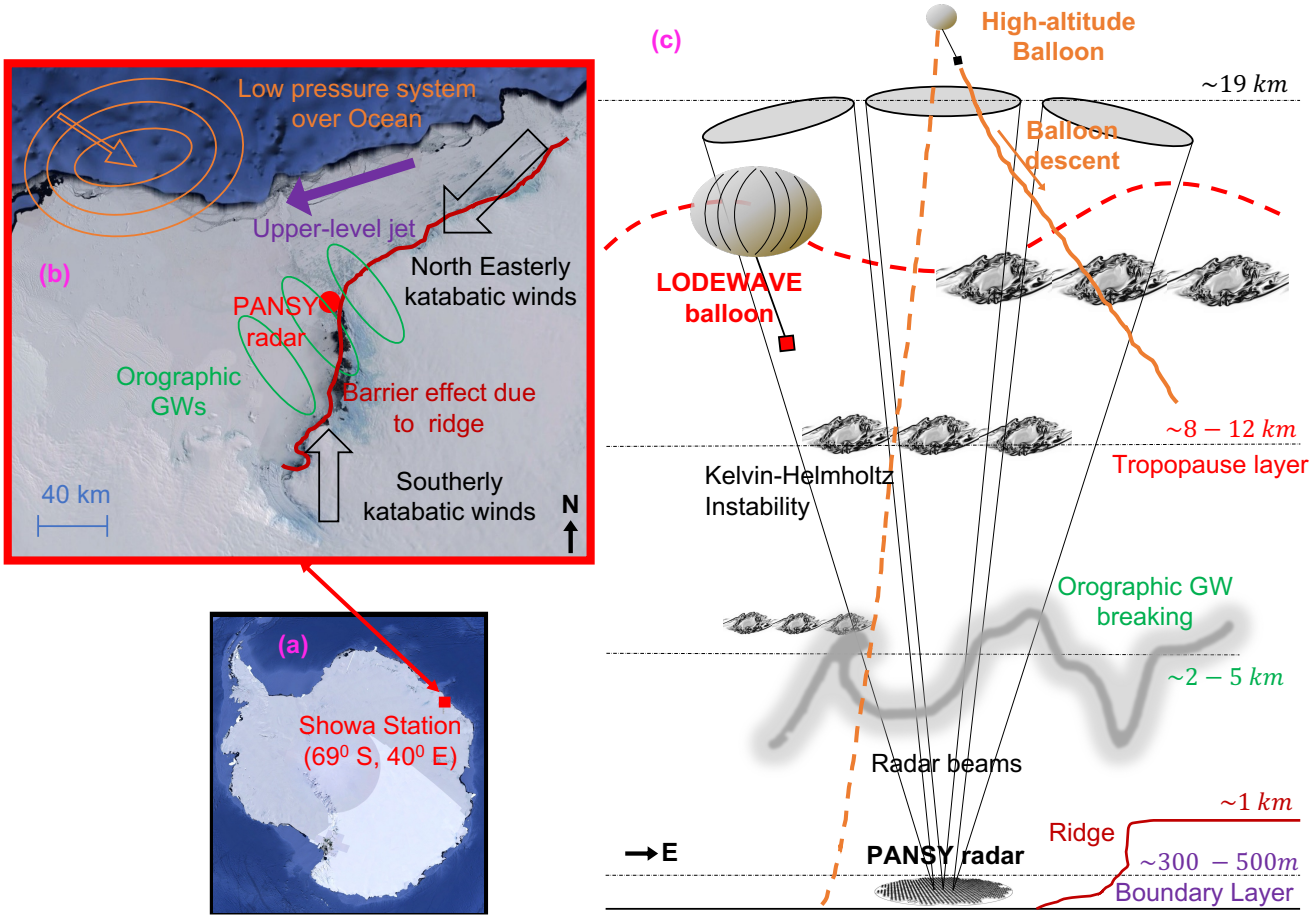

Figure 1: (a) Syowa Station and the Antarctic continent; (b) typical atmospheric processes occurring over Syowa station; (c) the proposed observation strategy.

Horizontal phase velocity analysis of gravity waves observed by OH arirglow imaging at Rio Gallegos, Argentina, near Andes

Takuji Nakamura[1,2] , Mitsumu K. Ejiri[1,2], Masaru Kogure[3], Septi Perwitasari[4], Yoshihiro Tomikawa[1,2], Masaki Tsutsumi[1,2], Akira Mizuno[5], Katsuhiko Tsuno[6], Takayo Ogawa[6], Satoshi Wada[6], and Jacobo Salvador[7] ,

[1]*National Institute of Polar Research (NIPR), Tachikawa, Tokyo, Japan*

[2]*Graduate University for Advanced Studies, SOKENDAI, Japan*

[3]*Faculty of Sceince, Kyushu University, Fukuoka, Japan*

[4]*NICT, Koganei, Tokyo, Japan*

[5]*ISEE, Nagoya University, Nagoya, Aichi, Japan*

[6]*RIKEN, RAP, Wako, Saitama, Japan*

[7]*National Scientific and Technical Research Council (CONICET), Santa Cruz, Argentina*

Atmospheric gravity waves are the key player of momentum and energy transport to the upper part of the middle atmosphere and lower thermosphere, and hence very important to understand the vertical couplings of the whole atmosphere from the ground to the thermosphere/ionosphere. Meteorological disturbances, topography, and jet stream instabilities generates gravity waves, which propagate vertically and horizontally. Recently, generation of the secondary gravity waves due to gravity wave breaking in the middle atmosphere has been recognized as a very important process because it plays a major role in transporting momentum and energy to the upper atmosphere, because it propagates efficiently beyond the MLT region to the thermosphere and ionosphere.

One of the hotspots for gravity waves is the Antarctic Peninsula and the Andes, where strong mountain waves are excited by tropospheric winds and topography. We have been conducting OH airglow imaging observations (altitude ~87 km) at Rio Gallegos (51.6S, 69.3W) in Patagonia, Argentina, near the Andes Mountains since late 2017. In this study, we report the characteristics of observed gravity waves by investigating horizontal phase velocity spectrum, i.e., the distribution of gravity wave energy in the 2D horizontal phase velocity region, observed in 2018.

In 2018, 138 nights of clear and no-moon images were acquired. The airglow images of Rio Gallegos were characterized by quasi-stationary waves, suggesting the influence of mountain waves, and wave breaking events, suggesting large wave amplitudes. These suggest that the Rio Gallegos site is located in an area of strong gravity wave activity originating from the Andes Mountains. These characteristics are similar to those observed by Pautet et al. (2021) at the Rio Grande (54S, 68W) during the winter season, but the frequency of quasi-stationary waves from our observations appears to be low.

We applied M-transform (Matsuda et al., 2014) to obtain horizontal phase velocity spectra of relative perturbation of airglow intensity pick up waves to the series of images without moon and clouds for the time windows longer than 120 min, for the one minute averaged images . The results for the wave components with periods of 5-60 min and horizontal wavelengths of 10-100 km showed that the spectra are very broad, up to 150 m/s, and that wind filtering (wind blocking) signals due to stratospheric zonal winds appear very frequently and clearly. In summer (November-February) the main propagation was eastward. In early winter (March-April) and late winter (August-October), phase speeds were faster/wider, with clear decrease of the energy for the phase speed within the wind blocking area. In midwinter, the spectral peak extends east-west near zero. Gravity wave energy (I'/I) is greatest around August-September and appears to be greater than at the Syowa station, where the late winter peak is less well-defined.

These observations suggest that the horizontal phase velocity spectrum analysis is an effective way for identifying the altitude range of gravity wave generation observed in the airglow layer at altitudes around 85-90 km.

References

Matsuda, T. S., T. Nakamura, M. K. Ejiri, M. Tsutsumi, and K. Shiokawa (2014), New statistical analysis of the horizontal phase velocity distribution of gravity waves observed by airglow imaging, Journal of Geophysical Research-Atmospheres, 119(16), 9707-9718, doi:10.1002/2014jd021543.

Statistical Study of Coincident Observations of Stratospheric Concentric Gravity Waves and Concentric Traveling Ionospheric Disturbances over the Continental U.S. in 2022

Masaru Kogure1,2,3, Jia Yue2,3, Min-Yang Chou2,3 , Huixin Liu1, Yuichi Otsuka4, Cora Randall5, Lars Hoffmann6, and Yuta Hozumi2,3

1 Department of Earth and Planetary Science, Kyushu University, Fukuoka, Japan.

2 NASA GSFC, 8800 Greenbelt Rd, Greenbelt, MD 20771, USA.

3 Catholic University of America, 620 Michigan Ave., N.E., Washington DC 20064, USA.

4 Institute for Space-Earth Environmental Research, Nagoya University, Nagoya, Japan.

5 Laboratory for Atmospheric and Space Physics, University of Colorado Boulder, Boulder, CO, USA

6 Jülich Supercomputing Centre, Forschungszentrum Jülich, Jülich, Germany

This study examines the seasonal distributions of concurrent stratospheric concentric gravity waves (GWs) observed by the Atmospheric Infrared Sounder (AIRS) and concentric traveling ionospheric disturbances (TIDs) detected by the ground-based GNSS-TEC network over the U.S. in 2022, aiming to illustrate mesoscale vertical coupling between the lower atmosphere and ionosphere. We compared these disturbances in the stratosphere and ionosphere with tropospheric weather conditions, including convective available potential energy (CAPE), extratropical cyclone center locations, and thermospheric background winds. Epicenters of the concentric TIDs associated with stratospheric concentric GWs were linked to areas with high CAPE over the central to eastern U.S. (~60–110°W) during summer, and over the southern U.S. (south of ~40°N) in spring and fall. In contrast, during fall, winter, and spring, epicenters over the northern U.S. (north of ~40°N) appeared south of regions with high extratropical cyclone activity, corresponding to cyclone centers. These findings suggest that convection was the primary source of concentric GWs driving TIDs over the continental U.S. throughout all four seasons, although the specific meteorological phenomena associated with convection varied by season. Convection in summer over the central to eastern U.S. and in spring over the southern U.S. could be linked to thunderstorms, whereas in fall through spring, convection over the northern U.S. may be triggered by warm and moist air advection linked to extratropical cyclones. In the fall, hurricanes over the North Atlantic Ocean could also induce convection. We also found that concentric TIDs were associated with 66% of the stratospheric concentric GW events, indicating that convection plays a significant role in generating TIDs in the lower atmosphere, contributing to vertical coupling between the lower atmosphere and ionosphere. Thermospheric winds affect the local time and horizontal distribution of concentric TIDs, with weaker winds during the day compared to nighttime, resulting in a higher occurrence rate of concentric TIDs during daytime.

An analysis of wind fields in the mesosphere at high latitudes in the Southern Hemisphere based on long-term PANSY radar observations

Eiji Tokimori, Masashi Kohma, and Kaoru Sato
Department of Earth and Planet Science, Graduate School of Science, The University of Tokyo

In the mesosphere, it is known that there is a residual mean circulation that consists of upwelling at high latitudes in the summer hemisphere, meridional flow toward the winter hemisphere, and downwelling at high latitudes in the winter hemisphere (Plumb, 2002). This meridional circulation is mainly driven by forcing due to absorption and breaking of gravity waves (McIntyre, 1989). Atmospheric tides are also known to contribute significantly to wind variations (e.g. Smith 2012). Meteor radar and MF radar observations are useful for the analysis of mean winds because they can provide continuous wind data for long periods in the mesosphere (e.g. Vincent, 1994; Dowby et al., 2007). In this study, we analyzed wind fields based on the long-term continuous observations by the PANSY radar at the Syowa Station (69°S, 40°E) (Sato et al., 2014), which is the first and only large atmospheric radar in the Antarctic, to reveal the seasonal variation of wind fields in the mesosphere at high latitudes in the Southern Hemisphere.

The PANSY radar provides winds estimated from turbulence echoes such as the polar mesosphere summer echoes (PMSE) and polar mesosphere winter echoes (PMWE) and those estimated from meteor echoes simultaneously. The standard observations, which use turbulence echo, provide 3-dimensional winds while the meteor observations provide horizontal winds. In this study, we used data based on the standard observations from October 2015 to May 2023 and the meteor observations from March 2021 to June 2023.

The meteor observations show that the zonal wind is westward (eastward) in summer (winter) below approximately z=97 km. In summer, the zonal wind changes from westward to eastward as the 0 m/s line gradually descends from z=95 km. A similar reversal of the zonal wind is observed in winter near z=97 km. The meridional wind is predominantly northward from December to February with a maximum at z=90-95 km. It is generally southward from April to October, but weaker than the northward wind in summer, with some periods of northward wind. The characteristics of zonal wind from the standard observations are consistent with those from the meteor observations. The maximum of the eastward wind from March to October is below z=70 km. The meridional wind is southward in winter below approximately z=65 km. The height of the 0 m/s line is near z=80 km except in March, April, September, and October. The vertical wind is downward below z=70 km and above z=90 km from April to November, but interestingly it is upward in the range of z=75-85 km from March to November. In summer, the vertical wind is negative in the range of z=80-95 km, possibly due to the descent of ice particles (i.e., polar mesospheric clouds). We will also show results of spectral analysis and hodograph analysis of gravity waves in the presentation.

References

Dowby, A. J., R.A., Vincent, M., Tsutsumi, K., Igarashi, Y., Murayama, W., Singer, and D. J., Murphy., 2007: Polar mesosphere and lower thermosphere dynamics: 1. Mean wind and gravity wave climatologies. *J. Geophys. Res.*, 112, D17104. doi:10.1029/2006JD008126.

McIntyre, M. E., 1989: On dynamics and transport near the polar mesopause in summer. *J. Geophys. Res.*, 94(D12), 14617-14628. doi:10.1029/JD094iD12p14617.

Plumb, R. A., 2002: Stratospheric transport. *J. Meteor. Soc. Jpn. Ser. II*, 80(4B), 793–809. doi:10.2151/jmsj.80.793.

Sato, K., M. Tsutsumi, T. Sato, T. Nakamura, A. Saito, Y. Tomikawa, K. Nishimura, M. Kohma, H. Yamagishi and T. Yamanouchi, 2014: Program of the Antarctic Syowa MST/IS Radar (PANSY), *J. Atmos. Solar-Terr. Phys.*, 118, PartA, 2-15. doi:10.1016/j.jastp.2013.08.022.

Smith, A. K., 2012: Global dynamics of the MLT. *Surv. Geophys.*, 33, 1117-1230. doi:10.1007/s10712-012-9196-9.

Vincent, R. A., 1994: Gravity-wave motions in the mesosphere and lower thermosphere observed at Mawson, Antarctica. *J. Atmos. Terr. Phys.*, 56(5), 593-602. doi:10.1016/0021-9169(94)90100-7.

Time variations of nitric oxide in the mesosphere and lower thermosphere over Antarctica associated with magnetic storms

Y. Miyoshi[1], A. Mizuno[2] , S.-I. Oyama[2], T. Nakajima[2], T. Nagahama[2], S. Nozawa[2], H. Goto[2], K. Hosokawa[2], K. Asamura[2], P. T. Verronen[3], R. Kataoka[4], N. Higashio[2], T. Mitani[2], T. Takashima[2], and I. Shinohara[2]

[1]*Nagoya University*, [2]*UEC*, [3]*Finnish Metelogical Institute,* [4]*JAXA,* [5]*NIPR*

Energetic electron precipitation leads to chemical consequences, particularly affecting the concentration of nitric oxide (NO) through the dissociation of molecular nitrogen caused by ion-pair production. An increase of NO in the mesosphere and upper stratosphere can be taken as an indicator of odd oxygen (Ox = O + O3) depletion by catalytic chemical reactions. Energetic electrons in the magnetosphere often increase during magnetic storms, suggesting that NO enhancement tends to occur during these events. In this study, we report the temporal variations in NO column density during magnetic storms at Syowa Station, Antarctica, and statistically investigate the average profile of NO column density. The observed temporal enhancements in NO column density are associated with both magnetic storms and seasonal variation. We conducted a superposed epoch analysis of NO column density around the minimum Dst index. The average variations show an increase in NO column density following the early recovery phase of storms. Since relativistic electron flux increases during the recovery phase of magnetic storms, the superposed epoch analysis suggests that an increase in energetic electrons in the radiation belts plays a key role in NO column density enhancement. This also suggest than there is likely an impact on mesospheric ozone is taking place during magnetic storms.

Comparison of frequency dependence of CNA due to various sources observed by spectral riometer

Tomotaka Tnaka[1], Yasunobu Ogawa[1,2], Yoshimasa Tanaka[1,2,3], Akira Kadokura[2,3], Mizuki Fukizawa[2], Kiyoka Murase[2], Keisuke Hosokawa[4], Shin-ichiro Oyama[2,5], Antti Kero[6,7]

[1]*The Graduate University for Advanced Studies, SOKENDAI*

[2]*National Institute of Polar Research, NIPR*

[3]*Joint Support-Center for Data Science Research, ROIS*

[4]*The University of Electro-Communications*

[5]*Institute for Space-Earth Environmental Research, ISEE*

[6]*Space Physics and Astronomy Research Unit, University of Oulu*

[7]*Department of Physical Sciences, University of Oulu, SGO*

A spectral riometer measures cosmic noise absorption (CNA) in the frequency between 20-55 MHz and is expected to have an ability to estimate the altitude profile of the electron density especially in the lower ionosphere. In the May 2024 solar magnetic storm event, spectral riometers in the arctic region; in Kilpisjärvi (KIL, 69.07°N 20.75°E) and in Oulujarvi (OUJ, 64.52°N, 27.23°E) etc., observed a number of CNA enhancements. During this event, the CNA enhancements were caused by three different sources: solar X-rays, solar energetic protons, and energetic electrons from the magnetosphere, known as major sources of ionization in the atmosphere. These three types of events may have different altitude profiles of ionization. The CNA is expected to be proportional to the -2 power of the observed frequency when the electron density enhancement occurs at higher altitudes (>70 km), while the CNA would be proportional to between -1 and -2 power of the frequency when the enhancement occurs at altitude lower than 70 km. Therefore, we will investigate the frequency dependence of these three types of the CNA events. At around noon on May 11, for example, an intermittent strong CNA was observed by the riometers, when an X-class solar flare occurred at 13:30 UT, and an increase of energetic proton (>10 MeV) flux was also measured by the GOES satellite. Note that the solar zenith at noon on the day at that location was 52.6 degrees. In the presentation, we will show how the frequency dependence of the CNA spectra differs between the three types of ionization agent, and then discuss the mechanism behind such dependencies.

Global analysis of cosmic-ray rigidity spectrum during extended Forbush decreases and its implications

[1] K. Munakata, [1] Y. Hayashi, [1] C. Kato, [2] M. Kozai, [3] R. Kataoka, [3, 4] A. Kadokura, [5] S. Miyake and the GMDN collaboration

[1]*Faculty of Science, Shinshu University, Nagano 390-8621, Japan*

[2]*PEDSC/ROIS-DS, Tachikawa, Tokyo 190-8518, Japan*

[3]*National Institute of Polar Research, Tachikawa, Tokyo 190-8518, Japan*

[4]*ROIS-DS/National Institute of Polar Research, Tachikawa, Tokyo 190-8518, Japan*

[5]*KOSEN Gifu College, Gifu, Motosu-city, 501-0495, Japan*

We present the global analysis of two extended decreases of the galactic cosmic ray intensity observed by world-wide networks of ground-based detectors in 2012. This analysis is capable of separately deriving the cosmic ray density (or omnidirectional intensity) and anisotropy each as a function of time and rigidity. A simple diffusion model along the spiral field line between Earth and a cosmic-ray barrier indicates the long duration of these events resulting from about 190 ° eastern extension of a barrier such as an IP-shock followed by the sheath region and/or the corotating interaction region (CIR). It is suggested that the coronal mass ejection merging and compressing the preexisting CIR at its flank can produce such the extended barrier. The derived rigidity spectra of the density and anisotropy both vary in time during each event period. In particular we find that the temporal feature of the “phantom Forbush decrease” reported in an analyzed period is dependent on rigidity, looking quite different at different rigidities. From these rigidity spectra of the density and anisotropy, we derive the rigidity spectrum of the average parallel mean-free-path of pitch angle scattering along the spiral field line and infer the power spectrum of the magnetic fluctuation and its temporal variation. Possible physical cause of the strong rigidity dependence of the “phantom Forbush decrease” is also discussed. These results demonstrate the high-energy cosmic rays observed at Earth responding to remote space weather. If time allows, we’ll also show comparisons with the neutron monitor’s Leader Fraction and the direct measurement of rigidity spectrum by AMS-02.

Astronomical observations at Dome Fuji II with Antarctic 30-cm submm telescope

Nario Kuno, Shunsuke Honda, Takuya Hashimoto [1, 2], Masumichi Seta, Naomasa Nakai[3], Kazuo Sorai, Dragan Salak [4], Hiroshi Matsuo, Tomofumi Umemoto, Makoto Nagai, Takafumi Kojima[5], and Antarctic astronomy consortium of Japan

[1]*University of Tsukuba*

[2]*Tomonaga Center for the History of the Universe*

[3]*Kwansei Gakuin University*

[4]*Hokkaido University*

[5]*National Astronomical Observatory of Japan*

1. Introduction

Antarctica plateau is the best site for submm-terahertz observations in Astronomy on the earth. Figure 1 shows the daily variation of precipitable water vapour (PWV) in Ridge A and the Chajnantor plateau in Chile where Atacama Large Millimeter/submillimeter Array (ALMA) was constructed. It is apparent that PWV in Ridge A is much lower and more stable than the ALMA site. Thanks to the low PWV, the transmission of the sky in Antarctic plateau is the best on the earth. Figure 2 shows the atmospheric transmission in Dome A, ALMA site and Mauna Kea. For the frequency higher than about 500 GHz, the transmission in Dome A is much higher than the ALMA site. Furthermore, Antarctic plateau is the only site on the earth where we can make observations at the frequency of > 1 THz. Taking the advantages of Antarctic plateau, we are conducting Antarctic 30-cm submm telescope project.

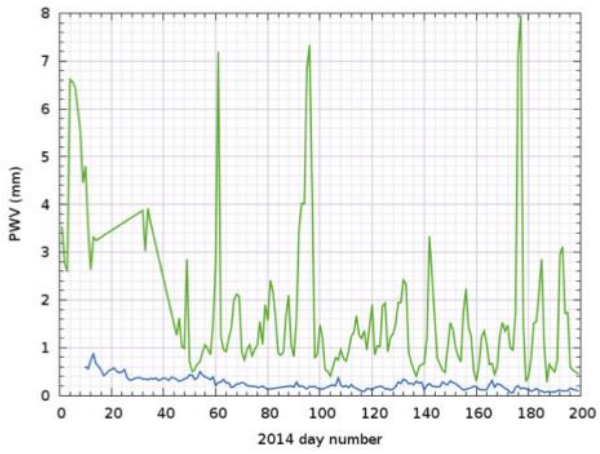

Figure 1 Precipitable water vapour measured at Ridge A, Antarctica (blue) and the Chajnantor plateau in Chile (green) (Burton et al. 2015).

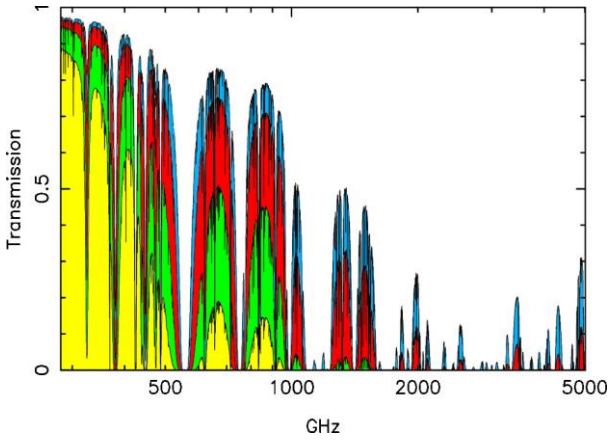

Figure 2 Comparison of atmospheric transmission. From top, the best tenth percentile at Dome A, 50% tile at Dome A, 50% tile at Atacama plain, 50% tile at Mauna Kea, respectively. (Yang et al. 2010).

2. Antarctic 30-cm telescope project

Cold molecular hydrogen H_2 (~10 K) is the main component of molecular clouds which is the site of star formation. However, H_2 at such low temperature cannot be observed directly since H_2 has no electric dipole moment. Therefore, CO(J = 1-0) line at 115 GHz is often used to trace molecular gas. CO molecule is, however, dissociated in diffuse gas due to FUV and cosmic rays. On the other hand, since the dissociation energy of H_2 is higher than that of CO, there are H_2 which remains in such regions but cannot be observed with the CO line. The missing molecular gas is called CO-dark gas.

[CI]($^3P_1$-$^3P_0$) (492 GHz), fine structure line of atomic carbon, is considered as a good tracer of the CO-dark gas. Recently, [CI]($^3P_1$-$^3P_0$) is also used as a molecular gas tracer for high-z galaxies. However, the observations of [CI]($^3P_1$-$^3P_0$) are limited so far. Therefore, to know the distribution and physical conditions of the molecular gas in the regions where [CI]($^3P_1$-$^3P_0$) is detected and the relation with molecular gas evolution, we need more detail observations in [CI]($^3P_1$-$^3P_0$) of molecular clouds in our Galaxy. In 500 GHz band, we can observe another important molecular emission line, CO(J = 4-3) (461 GHz). Since CO(J = 4-3) has a higher excitation energy and higher critical density than CO(J = 1-0), the line is a good tracer of warm and dense molecular gas associated with star forming regions.

We are conducting a project in which we will transport a 30-cm submm telescope (Fig. 3) to Dome Fuji II and make a Galactic plane survey in [CI]($^3P_1$-$^3P_0$) and CO(J = 4-3) using the telescope. The high transmission and stability of the

atmosphere in Dome Fuji II make us possible to conduct such large area mapping in these lines for the first time. We can observe about half of the Galactic plane with total observing time of about 1500 hours (Fig. 4). We have developed a sideband separated receiver using the wideband mixer developed for ALMA band 8 by National Astronomical Observatory of Japan. We can observe the two lines simultaneously with the wideband receiver. The 30-cm telescope is designed to use under the harsh Antarctic environment. For example, rubber heaters are attached to the motors. Since available power is limited in Antarctica, the power consumption of the telescope is kept small, less than 2.4 kW. For future upgrade to higher frequency, the optics of the telescope is designed to be frequency independent matching. Since the pointing source is very limited at 500 GHz band, we use an optical pointing system. Since we use the telescope during summer in Antarctica, the optical pointing system which can be used in daytime was developed. The beam size of 9' at 500 GHz is the same as the CO(J = 1-0) survey by Center for Astrophysics (CfA) (Dame et al. 2001), so that we can make a direct comparison with the lower excitation line of CO to investigate the physical properties of molecular gas. We will transport the 30-cm telescope to Dome Fuji II in 2026 and conduct the Galactic plane survey in [CI]($^3P_1$-$^3P_0$) and CO(J = 4-3) until 2029.

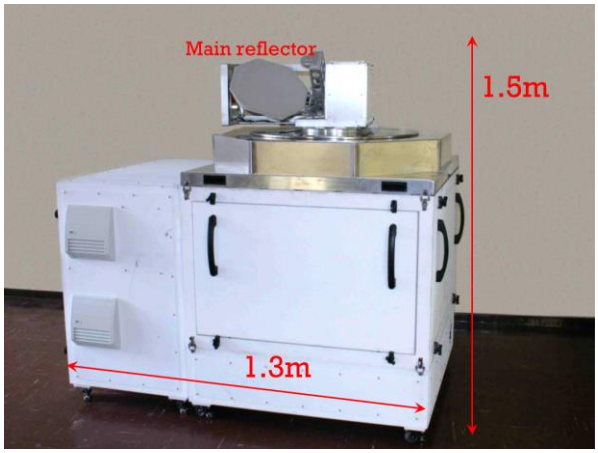

Figure 3. Antarctic 30-cm telescope. (Ishii et al. 2014)

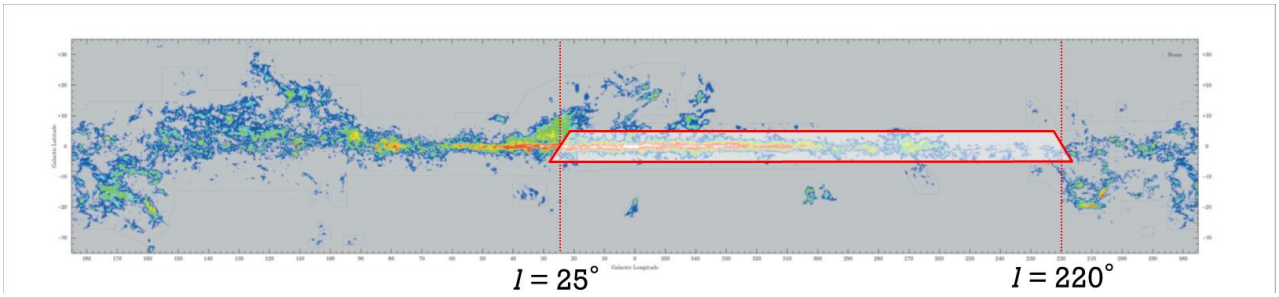

Figure 4. CO(J =1-0) map of the CfA (Center for Astrophysics) Survey (Dame et al. 2001). The mapping area of our survey is indicated by red lines. The survey of the region will be completed by ~1500 hours with the Antarctic 30-cm telescope

3. Future plan of Antarctic astronomy

As the next step following the 30-cm submm telescope project, we are plannig 12-m Terahertz telescope project. The telescope is designed to have very wide field of view for the survey of distant galaxies which can be found only with dust emission. MKID arrays with wide field of view will be installed for the survey. Heterodyne receivers whose observing frequencies are matched to the atmospheric windows upto 2 THz will be also installed. Observations of emission lines from atoms and molecules are important for accurately determining the distance to galaxies through redshift. It is also an effective means of investigating the physical state and radiation field of interstellar matter in distant galaxies by using many molecular emission lines and atomic fine structure lines that can be observed in THz band due to redshift.

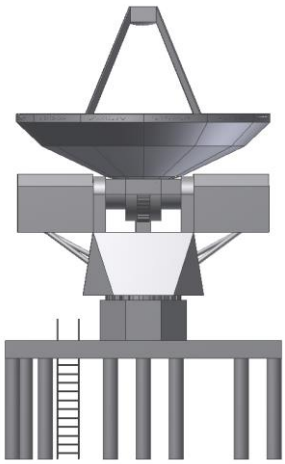

Figure 5. Schematic view of Antarctic 12-m THz telescope.

References

Burton, M. et al., Astronomy from the high Antarctic plateau, Pub. Korean Astron. Soc. 30, 611-616, 2015.

Dame, T. M. et al., The Milky Way in molecular clouds: a new complete CO survey, ApJ., 547, 792-813, 2001

Ishii, S. et al, Development of a 30-cm submillimeter-wave telescope for the operation at Dome Fuji in Antarctica, Proc. SPIE 9145, Ground-based and Airborne Telescopes V, 914535, 1-8, 2014

Yang,H. et al., Exceptional Terahertz Transparency and Stability above Dome A, Antarctica, Pub. Astron. Soc. Pacific. 122, 490-494, 2010.

Effects of asymmetric loss cone on wave-induced electron precipitation in a small magnetosphere

Mitsunori Ozaki[1], Takeru Kondo[1], Yuto Yamada[1], Satoshi Yagitani[1], Mitsuru Hikishima[2] and Yoshiharu Omura[3]
[1]*Kanazawa University, Kanazawa, Japan*
[2]*Magnedesign Corporation, Nagoya, Japan.*
[3]*Research Institute for Sustainable Humanosphere, Kyoto University, Uji, Japan.*

Mercury, the first planet from the Sun, has a small magnetosphere. In particular, Mercury has a large loss cone difference in both northern and southern hemispheres due to the northward shifted magnetic dipole. It is predicted that the asymmetric loss cones can affect the whistler instability by the effects of the asymmetric temperature anisotropy and the asymmetric Lorentz and mirror forces in the north and south polar regions. A large loss cone difference between hemispheres is exhibited in the Earth's South Atlantic Magnetic Anomaly (SAMA) region, similar to that of Mercury, but whistler-mode waves are not usually active in the SAMA region due to the dense cold electrons inside the Earth's plasmapause. In this study, we focus on the energetic electron precipitation through electron–whistler interactions in Mercury's small magnetosphere to understand the effects of the unique factor of the asymmetric loss cone. We simulate pitch angle scattering in two different cases for symmetric (the same loss cone size at the north and south polar regions) and asymmetric (an assumption of 10-deg. wider at the south polar region) bounce loss cones using a Particle-in-Cell code. In the simulation results, we see clear prompt electron precipitation events induced by whistler-mode waves in both cases. Moreover, the simulation result in the asymmetric loss cone case shows more active electron precipitation at the northern hemisphere in comparison with that for the symmetric loss cone, because the whistler instability in the southern hemisphere is enhanced by the effects of the larger loss cone. In this presentation, we will present the significant difference of the electron precipitation driven by the nonlinear whistler instability in the two hemispheres in Mercury's small magnetosphere.

Japanese Research Infrastructure for EISCAT_3D

Taishi Hashimoto[1], Yasunobu Ogawa[1], Yoshimasa Tanaka[1], Takanori Nishiyama[1], and Mizuki Fukizawa[1]
[1]*National Institute of Polar Research*

EISCAT_3D is an international research infrastructure consisting of three (or five in the final design) phased-array incoherent-scatter radars in the northmost areas of Norway, Finland, and Sweden. The radar system will cover vast research fields, including studies of the atmosphere and near-Earth space environment, the solar system and radio astronomy, space weather forecast, and space debris monitoring. The EISCAT_3D is now in its construction phase.

In conjunction with the progress of the EISCAT_3D project, the Advanced Radar Research Promotion Center (ARRC) at NIPR is also preparing its research infrastructure for data management and custom analysis of the data products of EISCAT_3D while referring to the one at the EISCAT_3D HQ. We have developed a new gateway system for the Japanese EISCAT_3D data and analysis. This gateway system has a user authentication system that we can fully control the accessibility to our data/service of each user, source code repository, package/container registries, an online user-computing platform based on the modern notebook style, and a huge storage system as a backup of the main database of the EISCAT_3D enhanced with custom analyses unique to Japan.

In this presentation, we introduce the current status of the Japanese research infrastructure for the EISCAT_3D and the plan for its future development.

Statistical analysis of pulsating auroras and ducted chorus waves

Yuri Ito[1,2], Yasunobu Ogawa[1,2,3], Yoshimasa Tanaka[1,2,3], Akira Kadokura[2,3], Mizuki Fukizawa[2], Keisuke Hosokawa[4], Yoshizumi Miyoshi[5], Tomoaki Hori[5], Yoshiya Kasahara[6], Shoya Matsuda[6] and Iku Shinohara[7]
[1]*The Graduate University for Advanced Studies, SOKENDAI*
[2]*National Institute of Polar Research*
[3]*Research Organization of Information and Systems, Joint Support-Center for Data Science Research*
[4]*University of Electro-Communications*
[5]*Institute for Space-Earth Environmental Research, Nagoya University*
[6]*Kanazawa University*
[7]*Institute of Space and Astronautical Science, JAXA*

Pulsating auroras (PsA) are considered to be caused by precipitation of a few to a few tens of keV electrons. The energetic electrons are scattered by lower-band chorus (LBC) waves, which are one of the whistler-mode waves in the magnetosphere, through the cyclotron resonance. Past study has suggested that, during PsA, relativistic electrons causing ozone depletion simultaneously precipitate into the ionosphere [Miyoshi et al., 2021]. Observational studies also suggested that, relativistic/sub-relativistic electrons precipitate to lower altitudes when PsA has a patchy structure and that PsA patches tend to develop towards the morning side [Tesema et al., 2020; 2022]. Our previous study proposed that the relationship between the shape of PsA and the energy of precipitating electrons is controlled by presence of magnetospheric density ducts and associated high-latitude propagation of chorus waves [Ito et al., 2024]. However, the background mechanism of how density ducts are generated, and the universality of the proposed model have not been clarified yet.

In order to understand the detailed development process of density ducts and quantitatively evaluate the universality, we are in the progress of a statistical analysis of PsA patches simultaneously observed by the multipoint optical instruments in the northern Europe and the Arase satellite. The survey period is from March 2017 to March 2024. We count the appearance of patches at the footprint of Arase as a single sample and investigate the spatiotemporal development of PsA patches, propagation latitudes of chorus waves. In this presentation, we will report the details of the analysis method, the observed data, and the initial results and discuss the statistical relationship between the PsA morphology and ducted propagation of chorus waves.

References

Miyoshi, Y. et al., Penetration of MeV electrons into the mesosphere accompanying pulsating aurorae, Scientific reports, 11, 2021.
Tesema, F. et al., Observations of electron precipitation during pulsating aurora and its chemical impact. Journal of Geophysical Research: Space Physics, 125(6), 2020.
Tesema, F. et al., Types of pulsating aurora: Comparison of model and EISCAT electron density observations. Annales Geophysicae, 40, 1–10, 2022.
Ito et al., On the Factors Controlling the Relationship Between Type of Pulsating Aurora and Energy of Pulsating Auroral Electrons: Simultaneous Observations by Arase Satellite, Ground-Based All-Sky Imagers and EISCAT Radar, Journal of Geophysical Research: Space Physics, 129, 2024.

On the precipitating electron energy of pulsating aurorae with and without internal modulations

Kiyoka Murase[1], Takanori Nishiyama[1], Mizuki Fukizawa[1], Ryoichi Fujii[1], Masaki Tsutsumi[1], Kaoru Sato[2] and Ryuho Kataoka[1]

[1]*National Institute of Polar Research*

[2]*The University of Tokyo*

Pulsating aurora is a major type of diffuse aurora, characterized by quasi-periodic pulsations in brightness ranging from a few seconds to several tens of seconds. They sometimes coexist with shorter-period variations of a few Hz, so called "internal modulations." The hierarchy of these periods has been observationally shown to correspond to the intensity variations in chorus wave which is responsible for electron precipitation causing pulsating aurorae. However, the number of reports on internal modulation is limited due to the high sampling rates (>10 Hz) required for optical observations to investigate internal modulation. The factors controlling the presence or absence of internal modulation has not been well understood.

This study aims to statistically investigate how the presence of internal modulation is controlled in the magnetosphere, and how this results in differences in the characteristics of energy of the precipitating electrons. This has been made possible by the recently published dataset of 10-Hz sampling images obtained by the High-speed Auroral Imaging (HAI) system at Syowa Station. We first tried frequency filtering to determine the timings and regions with internal modulations for an example dataset. It is confirmed that a simple way of subtracting the running average from the original auroral intensity shows enough performance to detect the modulation. This method of detecting internal modulation is applied to a three-year data set from 2017 to provide a statistical view of the internal modulation. We will discuss differences in the energy spectra of precipitating electrons causing pulsating aurora with/without the internal modulation based on the atmospheric ionization profiles obtained by an imaging riometer and the PANSY radar at Syowa Station.

Acknowledgement: The observations at Syowa Station were mainly supported by the Research Program of Japanese Antarctic Research Expedition (JARE) of the MEXT. The redistribution of the imaging riometer data has been done by Dr. Yoshimasa Tanaka.

Long-term variations and trends in the polar E-region: An update

Lindis Merete Bjoland[1]and Yasunobu Ogawa[1]
[1]*National Institute of Polar Research*

As the EISCAT UHF radar system in Northern Scandinavia started its operations in the early 1980s, the collected data covers several solar cycles. Bjoland et al (2017) investigated long-term variations and trends in the peak altitude of the Hall conductivity and the ion temperature around noon using data from 1981-2015. Their results indicated a weak descent (~0.2 km/ decade) in the peak altitude of the Hall conductivity and a cooling trend (~10 K/ decade) in ion temperature at 110 km, after adjusting for seasonal and solar cycle dependence. However, other factors than solar zenith angle and solar activity also influence the ion temperature at this altitude and a further investigation of these factors are necessary to derive a conclusive trend.

We present an update using EISCAT database from 1981-2023 to investigate how the trends in the E-region have evolved since the previous study. Preliminary results indicate a consistent trend in the peak altitude of the Hall conductivity (~0.2 km/decade), while no significant trend can be seen in the ion temperature at 110 km altitude. However, the trend in ion temperature over Tromsø using the IRI model over the same period and at the same altitude shows a clear cooling trend of about 3 K per decade. In this paper we discuss the updated findings and explore the ion temperature trend at different E-region altitudes.

Optical manifestations of cold dense plasma sheet and super dense plasma sheet: optical and radar observations in Tromsoe and Skibotn, Norway

Keisuke Hosokawa[1], Yasunobu Ogawa[2], Masaki N. Nishino[3], Yoshizumi Miyoshi[4], Kanako Seki[5], Mizuki Fukizawa[2], Sota Nanjo[6], and Shin-Ichiro Oyama[4]

[1]*The University of Electro-Communications, Tokyo, Japan*

[2]*National Institute of Polar Research, Tokyo, Japan*

[3]*Institute of Space and Astronautical Science/Japan Aerospace Exploration Agency, Kanagawa, Japan*

[4]*Institute for Space–Earth Environmental Research, Nagoya University, Nagoya, Japan*

[5]*The University of Tokyo, Tokyo, Japan*

[6]*Swedish Institute of Space Physics, Kiruna, Sweden*

Here, we present a distinctive sequence of auroral phenomena observed on the night of November 12-13, 2023, in Tromsø and Skibotn, Norway. Initially, a faint reddish aurora appeared in the pre-midnight sector, persisting for over four hours. This prolonged period of extremely low-energy electron precipitation occurred without any substorm activity. During the latter half of this interval, the EISCAT UHF radar detected intense ionization in the F region (above 200 km), consistent with the continued presence of the faint reddish aurora at high altitudes. Following this extended period, an exceptionally bright greenish aurora emerged, marking the onset of a substorm characterized by a significantly higher flux of precipitating electrons than usual.

Throughout the faint reddish aurora, the interplanetary magnetic field (IMF) remained strongly northward, shifting southward just before the appearance of the bright greenish aurora. Prolonged northward IMF conditions often correlate with the presence of cold and dense plasma in the plasma sheet, known as the cold dense plasma sheet (CDPS: e.g., Terasawa et al., 1997). The plasma density and temperature in the CDPS are influenced by the solar wind during these northward IMF periods, indicating the solar wind as the plasma source for the CDPS. The faint reddish aurora observed on the evening of November 12, 2023, may represent the first ground-based optical evidence of CDPS in the magnetotail at auroral latitudes. We hypothesize that the CDPS formed during the extended northward Bz period from approximately 14 UT on November 12, without any substorm activity. The sudden southward turning of IMF around 24 UT likely triggered the substorm, releasing the well-accumulated cold and dense plasmas in the plasma sheet, which may be regarded as a signature of the superdense plasma sheet (e.g., Borovsky et al., 1997). Such a combination of prolonged northward Bz and the subsequent southward shift in the IMF appears to have resulted in a unique auroral display. The sequential occurrence of faint reddish and bright greenish auroras suggests that ground-based optical observations in the auroral zone can serve as a diagnostic tool for identifying the formation of CDPS and the subsequent release of dense plasmas stored in the magnetotail.

References

Terasawa, T., et al. (1997), Solar wind control of density and temperature in the near-Earth plasma sheet: WIND/Geotail collaboration, Geophys. Res. Lett., 24, 935.

Borovsky, J. E., M. F. Thomsen, and D. J. McComas (1997), The superdense plasma sheet: Plasmaspheric origin, solar wind origin, or ionospheric origin?, J. Geophys. Res., 102, 22,089–22,097, doi:10.1029/96JA02469.

Roles of plasma sheet flow and the M-I coupling convection in reproducing the substorm with the global simulation

グローバルシミュレーションでサブストームを再現する場合の プラズマシート対流と M-I 結合の役割

T. Tanaka[1]
[1] *REPPU Code Institute*

The substorm is reproduced from the REPPU global simulation. A quasi-steady state is generated under the northward IMF, and then the IMF is reversed to southward to generate the substorm. In the initial state, earthward flow is given to the plasma sheet, which results in the formation of the thick plasma sheet. The thinning progresses rapidly during the growth phase, and just before the onset, the flux rope, the NENL, and the plasmoid are generated from near earth to far from the earth. With the initial condition that considers plasma sheet earthward flow, the NENL is formed in the mid-tail, not in the near-earth tail. The mid-tail NENL and the BBFs that start from there form DFs. The DF proceeds toward the dipolar region. After the first DF reaches the near-earth region, the onset FAC and the WTS appear, but the CW is not generated. The onset signature depends on the distribution of plasma sheet dissipation. Not only the formation of the flux rope in the near-earth tail but also the generation of the NENL in the mid-tail require the coupling of ionospheric convection to magnetospheric convection. Tailward flow associated with the flux rope is overwhelmed by earthward NENL flow, and eventually the whole feature appears the outside-in. Finally, the onset appears to coincide with the arrival of flow from the NENL.

サブストームのグローバルシミュレーションを行う。IMF 北で準定常状態を作成し、IMF を南に反転させ、サブストームを生成する。初期状態では、プラズマシートに①地球向き流を与え、これにより厚いプラズマシートが形成される。成長相の thinning は急激に進行し、オンセット直前には、地球の近くから遠くに向けて、フラックスロープ、NENL、プラズモイドが形成される。地球向き流を考慮した初期条件では、NENL は近尾部でなく中尾部で形成される。中尾部 NENL と、そこから出発する BBF は、DF を形成しつつ近尾部に至る。DF の近尾部への到達後、オンセット FAC、WTS が再現されるが、しかし CW は生成されない。オンセットの様相は、②プラズマシート散逸の分布に依存する。中尾部の NENL の形成、近尾部のプラックスロープ発生には、共に③磁気圏対流に電離圏対流が結合することが必要である。フラックスロープに伴うテイル向き流は、地球向きの NENL 流に圧倒され、最終的に全体は outside-in に見える。最終的には、オンセットは NENL からのフローの到達に一致するように見える。

AI emulator and data assimilation of auroral current system

Ryuho Kataoka[1], Sachin Reddy[1], Shinya Nakano[2], Shigeru Fujita[2], and Aoi Nakamizo[3]
[1]*NIPR*
[2]*ISM*
[3]*NICT*

We are developing a new AI emulator and data assimilation models of the auroral current system in the northern and southern polar regions. First, the accuracy of the emulator SMRAI2 (Kataoka et al., 2004) was improved. That is SMRAI2 plus, skipping the Principal Component Aanalysis part. Further development, SMRAI3, is ongoing based on the deep learning technique called Long-Short Time Memory using a huge data set of REPPU simulation results as conducted at NICT for several years. We will report the latest situation, including the data assimulation with SuperDARN data using SMRAI2 plux, and the use of field-aligned current data of AMPERE project via the deep learning technique for comparison with SMRAI2.

References

Kataoka, R., Nakamizo, A., Nakano, S., & Fujita, S. (2024). Machine learning-based emulator for the physics-based simulation of auroral current system. Space Weather, 22, e2023SW003720. https://doi.org/10.1029/2023SW003720

A Comprehensive Geometric Description of Time-Evolving Magnetic Fields via Magnetic Frenet-Affine Connection

Akimasa Yoshikawa[1]
[1]Department of Earth and Planetary Science, Kyushu University
[1]International Research Center for Space and Planetary Sciences (i-SPES), Kyushu University

To analyze the magnetic vector field as a collection of densely distributed magnetic field lines, we have developed a novel connection framework on a manifold. This framework is characterized by the following features:

1. Description of Individual Magnetic Field Lines: Each magnetic field line $\mathbf{r}_T$ is described using the Frenet moving frame {**T**, **N**, **B**}, where **T** is the tangent vector of the magnetic field line, **N** is the normal vector, and **B** is the binormal vector. The directional changes of {**T**, **N**, **B**} along the magnetic field line $\mathbf{r}_T$ are described by Affine connection coefficients, which are combinations of the curvature and torsion of the curve $\mathbf{r}_T$. The geometric properties of each individual magnetic field line are uniquely determined by the distribution of these connection coefficients. The {**T**, **N**, **B**} frame distributed along each magnetic field line densely fills the manifold, reflecting the dense distribution of magnetic field lines.

2. Connecting Adjacent Magnetic Field Lines: To connect adjacent magnetic field lines using the moving frame, we introduce coordinate curves $\mathbf{r}_N$ with **N** as the tangent vector and $\mathbf{r}_B$ with **B** as the tangent vector. The directional changes of {**T**, **N**, **B**} along the coordinate curve $\mathbf{r}_N$ are described by affine connection coefficients corresponding to small displacements in the N direction, while the directional changes of {**T**, **N**, **B**} along the coordinate curve $\mathbf{r}_B$ are similarly described by affine connection coefficients. Thus, the relative directional changes between adjacent magnetic field lines are fully captured by the curvature and torsion of the coordinate curves $\mathbf{r}_N$ and $\mathbf{r}_B$.

3. Global Network of Local Coordinate Systems: The local coordinate system {**T**, **N**, **B**}, distributed along the coordinate curves, forms a network across the entire space through the connections along these curves. The geometric structure of the magnetic field is fully reproduced by the torsion and curvature of each coordinate curve. The local coordinate system network constructed by this connection framework serves as a generalized coordinate system on magnetic fields with any geometric structure.

The current flowing through this network, based on Ampère's law, generates shear in the magnetic flux density, controlling the curvature of the magnetic field lines and creating field torsion. Faraday's law induces fluctuations throughout the network via changes in the direction of **T** as the magnetic flux density changes over time. Since this coordinate system locally forms a Euclidean space, vector analysis performed within this framework considers not only the partial derivative information of the components but also the rate of change of coordinates projected onto the Euclidean space. Furthermore, by using the connection coefficients obtained through the procedures described in points 1 and 2, we can determine the Cartan connection 1-forms and derive the first and second structure equations, allowing us to formalize the geometric structure inherent in our proposed connection framework.

By conceptualizing the structure of the magnetic field as a collection of densely distributed magnetic field lines and connecting each magnetic field line, described using the Frenet frame, to coordinate curves expanding in the direction perpendicular to the magnetic field lines using affine connection, we have successfully formulated a generalized magnetic field coordinate system that evolves over spacetime. In this presentation, we will introduce the details and utility of this framework.

Preliminary results of LODEWAVE Phase II (LOng-Duration balloon Experiment of gravity WAVE over Antarctica)

Yoshihiro Tomikawa[1,2,3], Kaoru Sato[4], Yoshitaka Saito[5], Isao Murata[6], Naohiko Hirasawa[1,2,3], Masashi Kohma[4], Kyoichi Nakashino[7], Daisuke Akita[8], Takuma Matuso[9], Masatomo Fujiwara[10], Takana Kaho[11], Lihito Yoshida[2], and Rina Kawakami[9]

[1]*National Institute of Polar Research*

[2]*The Graduate University for Advanced Studies, SOKENDAI*

[3]*Polar Environment Data Science Center, Research Organization of Information and Systems*

[4]*The University of Tokyo*

[5]*Japan Aerospace Exploration Agency*

[6]*Tohoku University*

[7]*Tokai University*

[8]*Tokyo Institute of Technology*

[9]*Meiji University*

[10]*Hokkaido University*

[11] *Shonan Institute of Technology*

The second observation campaign of LODEWAVE (LOng-Duration balloon Experiment of gravity WAVE over Antarctica) was conducted at Syowa Station, Antarctica from January to February 2024. Based on the results of the first observation campaign, in which the flight duration was less than 3 days, we improved the balloons and succeeded in releasing two new balloons, but the flight duration was less than 3 days in both cases. In this presentation, we will report the results of the preliminary analysis of the data obtained from this observation and our future plan.

Test observation of simultaneous and common-volume Ca/Ca$^+$ with a new resonance scattering lidar

Mitsumu K. Ejiri[1,2], Masayuki Katsuragawa[3], Ayaka Hashimoto[3], Sota Kobayashi[3], Sayako Miyoshi[3], Takuo T. Tsuda[3], Takuji Nakamura[1,2]

[1]Natianl Institute of Polar Research, [2]SOKENDAI, [3]The University of Electro-Communications

In a transition region between neutral atmosphere and geospace plasma (80 - 500 km), the vertical mass transport process has still to be revealed because simultaneous measurement of neutral atmosphere and plasma is quite difficult. There are layers of metal atoms and ions produced by meteoric ablation in the mesosphere and lower-thermosphere region. The meteoric ablation occurs mainly around 80-120 km, so metal layers are usually observed below 120 km. However, there have been many recent reports confirming the presence of metal atoms at altitudes higher than that by resonant scattering lidar observations. A simulation study conducted by Chu and Yu (2017) to investigate a possible source of thermospheric iron layers observed at McMurdo Station in Antarctica suggested that metal atoms may be incorporated into vertical transport in geospace with ionization and neutralization, moving over a wide altitude range. Simultaneous observation of the vertical density profiles of metal atoms and ions and tracking their temporal changes could provide observational evidence of large-scale vertical mass transport in the transition region. Calcium is the only metal that can be observed in both atom (Ca) and ion (Ca$^+$) by ground-based resonant scattering lidar observations. To measure simultaneous and common-volume density profiles of Ca/Ca$^+$, as a dynamical tracer in this region, we are developing a resonance scattering lidar system, which has an injection-locked Ti:Sapphire laser; a multi-frequency, nanosecond pulse, and a broad frequency tenability. We succeeded a test observation of Ca/Ca$^+$ by the new lidar system with simultaneous 2-fequency oscillation on September 5, 2024. In this presentation, we will explain current status of development and show a preliminary result of test observation.

References

Chu, X., and Z. Yu (2017), Formationmechanisms of neutral Fe layers in thethermosphere at Antarctica studiedwith a thermosphere-ionosphere Fe/Fe$^+$(TIFe) model,J. Geophys. Res. SpacePhysics,122, 6812–6848, doi:10.1002/2016JA0237

OSp3

A Ground-based observation of spectra of noctilucent clouds with a compact spectrometer

Ayune Masuda[1], Akiho Endo[1], Peter Dalin[2] and Hidehiko Suzuki[1]
[1]*Meiji University*
[2] *Swedish Institute of Space physics*

Noctilucent Clouds (NLCs) are ice clouds that appear mainly in sub-polar regions (50 degrees - 60 degrees in latitude) during the summer season of both hemispheres. The typical altitude of NLCs is known to be 80 – 90 km. This ice cloud provides a lot of information about the mesopause region and is regarded as one of the important tracers of this region. The occurrence and distribution of NLCs give the activity of the atmospheric waves of various scales and these might be a signature of global changes such as the effects of global warming and giant volcanic eruptions. The imaging technique is the most common method to observe NLCs since even ordinal digital cameras can easily capture detailed features of NLCs. A Spectropic observation is also an effective method to study NLCs since it provides information about the physical properties of the ice cloud (e.g. particle sizes, shape, and size distribution). A Recent progress in the development of sensitive and low-cost sensors allows us to easily introduce the spectroscopic observation of NLCs as well as the imaging method.

We have developed a compact spectrometer which consists of imaging lenses, a transmitting grating, a slit, and a CMOS sensor (Figure 1). The housing is made from a PLA filament and printed out with a 3D printer. The color camera for f.o.v checking (f.o.v camera) is fixed on the top of the housing. The direction of the center f.o.v of this camera is aligned to be parallel to that of the spectrometer. The correspondence of the f.o.v of the spectrometer along the slit and the region in the image from the f.o.v camera is known by a calibration. Thus, we have knowledge from which region of the image the spectrum is acquired. The spectrometer is fixed on the motorized rotating stage. This stage is controlled from a laptop computer, modifying the azimuthal direction of the f.o.v to chase the motion of NLCs. The spectrometer was operational between August 15th and 22nd in Kiruna (67.86N, 20.42E), Sweden, in 2024 for a test NLC observation. Fortunately, we successfully observed the NLCs by the spectrometer on the night of 19 to 20 August during the test observation. The NLCs captured on this night continuously appeared for 2.5 hours. We could chase the motion of the NLC by using the rotating stage and thus, successfully acquired the NLC spectra with various scattering angles relative to the Sun position. The images of the NLC are also captured by the f.o.v camera. This enables us to deduce the motion of the NLC (i.e. direction and speed of the horizontal wind at the mesopuase region). We will report the results of the initial analysis of the test observation in this presentation and discuss the scientific possibility realized by the simultaneous observation of NLCs with the camera and the spectrometer.

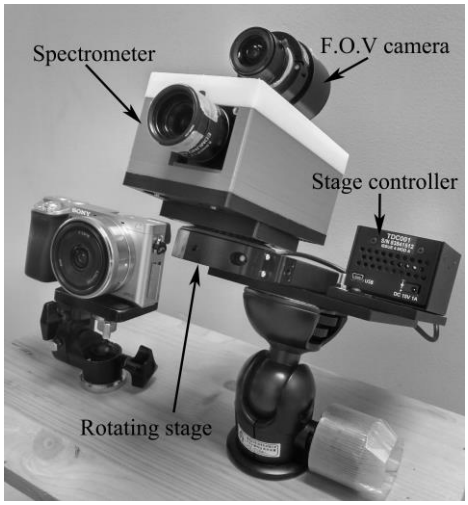

Figure 1. An appearance of the compact spectrometer.

NLC Imager for observations in the high latitude region. -The test observation in Kiruna, Sweden

Akiho Endo[1], Rina Kawakami[1], Ayune Masuda[1], Peter Dalin [2], Takuo Tsuda[3] and Hidehiko Suzuki[1]
[1]*Meiji University*
[2]*Swedish Institute of Space physics*
[3]*University of Electro-Communications*

Noctilucent cloud (NLC) images often contain fine wavy structures ranging from several kilometers to several tens of kilometers. These are thought to reflect local small-scale atmospheric disturbances in the upper mesosphere. Satellite imaging data cannot resolve such fine structures, and thus, ground-based imaging of NLCs is the effective method to study the small-scale disturbances in the upper mesosphere.

NLCs are frequently observed by satellites (e.g. AIM satellite) in the high-latitude regions. However, this area is under the influence of the midnight Sun, which makes it difficult to detect NLCs from the ground because of the bright background sky condition. Therefore, opportunities for NLC observations from the ground in the high-latitude regions are limited. On the other hand, there is an opportunity for NLC observations during the NLC decline period (August) even in the high latitude region. In addition, slow variations in the solar elevation angle enables continuous observation of NLCs with similar geometric conditions throughout nights in August. Thus, there is evident merit in studying the NLC morphology if the probability for NLC observations increases in the high-latitude regions.

We have examined the feasibility of overcoming this “bright background sky problem” by developing an optical imager dedicated to noctilucent cloud observations [Nakamura et al.,2021]. Noctilucent clouds are known to have a spectral peak in their radiance at 400-500 nm [Lange et al.,2022]. On the other hand, the background spectrum in twilight sky attenuates in wavelengths shorter than 680nm. Therefore, there should be an optimum wavelength band for noctilucent cloud observations which gives a better signal-to-noise ratio (SNR) in shorter wavelength regions. In this study, the most suitable bandpass for NLC observations is considered based on the ground spectra of the twilight background sky obtained in the polar region. We propose a new imaging technique which is based a cooled CMOS camera equipped with a bandpass filter, having the center wavelength at 371 nm and 40nm bandwidth. Using his new technique one can obtain an effective SNR (SNR>1.80) for NLC under a bright sky condition which corresponds to a local solar zenith angle of ˜91°.

We carried out the first test observation of the developed imager in Kiruna, Sweden (N 67.8, E20.4) in August 2024. Bright noctilucent clouds were registered with the NLC imager, the digital camera, and the small spectrometer between 21:05 and 23:25 on 19 August 2024 (UTC). A preliminary result of this test observation by the three instruments is presented. We discuss the performance of our new camera based on the SNR of the NLC images by comparing the NLC spectra simultaneously obtained with our spectrometer to the previous research [e.g. Fogle and Rees,1972].

References

Nakamura et al., sgepss , 2021.

Lange, A., Baumgarten, G., Rozanov, A., & von Savigny, C. (2022). On the color of noctilucent clouds. Annales Geophysicae,40(3), 407–419.https://doi.org/10.5194/angeo-40-407-2022

Fogle, B., & Rees, M. H. (1972). Spectral measurements of noctilucent clouds.Journal of Geophysical Research,77(4), 720–725. https://doi.org/10.1029/ja077i004p00720

Study of OH Airglow Intensity Variation During an Active Aurora Event

Satoshi Ishii[1], Hidehiko Suzuki[2], Yoshimasa Tanaka[3, 4, 5], Masaki Tsutsumi[4, 5], Makoto Taguchi[1], Mitsumu K. Ejiri[4, 5], Takanori Nishiyama[4, 5], Akira Kadokura[3, 4,]

1. Rikkyo University, 2. Meiji University, 3. Research Organization of Information and Systems Joint Support-Center for Data Science Research, 4. National Institute of Polar Research, 5. SOKENDAI

We report the results of OH (8-4) airglow observations at Syowa Station over 12 years. We conducted ground-based spectral observations of OH (8-4) airglow emitted from the mesopause region at Syowa Station during the winter seasons from February 2008 to October 2019. These observations have been carried out again since 2021. We derived the rotational line intensities of the OH (8-4) band (OH intensity) and the corresponding rotational temperatures.

We observed distinct intensity variations occurring over periods ranging from several tens of minutes to several hours. These variations differed from the sinusoidal patterns typically caused by atmospheric gravity waves, which are often seen in mid-latitude regions. Suzuki et al. (2010) detected only one such event from observations in 2008, but several similar events were detected in subsequent observations. This suggests that OH intensity fluctuates due to changes in the atmospheric composition of the polar mesopause associated with energetic particle precipitation (EPP), a phenomenon unique to the polar regions.

The OH molecule becomes excited through an exothermic reaction between an ozone molecule and atomic hydrogen. It is believed that EPP into the upper atmosphere produces NOx and HOx, which subsequently lead to destruction of ozone molecules. Thus, the OH intensity is believed to fluctuate due to changes in the atmospheric composition of the polar mesopause associated with EPP.

We extracted EPP events from cosmic radio noise absorption (CNA) data obtained through the imaging riometer observations at Syowa Station, defining an EPP event as starting when the CNA level was over 1.0 dB. Additionally, image data captured by the color digital cameras at Syowa Station were used to check auroral activities. Analysis of these data suggests that some events of the OH intensity variations occurring within a few hours appear to be correlated with the temporal development of auroral substorms. The OH intensity increases before EPP events, decreases afterward, and also decreases when the aurora becomes active.

In this presentation, we will show the temporal variations in OH intensity that are linked to auroral activities observed at Syowa Station between 2016 and 2022. Furthermore, we will discuss the impact of EPP in the polar mesopause regions.

References

Suzuki et al., The increase in OH rotational temperature during an active aurora event, Ann. Geophys., 28, 705–710, 2010.

High spatial and temporal resolution wind observations based on network MF radar meteor echo measurements

Masaki Tsutsumi[1], Toralf Renkwitz[2], Jorge L. Chau[2], and Juha Vierinen[3]
[1]*National Institute of Polar Research, Japan.*
[2]*Leibniz Institute of Atmospheric Physics, Germany*
[3]*The Arctic University of Norway, Norway*

MF radar meteor wind measurements have been made at Syowa station (69S, 39E) since 1999 [Tsutsumi and Aso, 2005]. A major improvement has further been made recently by fully scrutinizing the nature of radio meteor echoes. The redeveloped technique shows that horizontal wind velocities can be estimated with a highly improved time resolution of about 10 minutes in the height region of 80-115 km, and can even be resolved horizontally every 50 km or so within the 10 minutes at around 90 km, the centroid height of meteor echo distribution. Such resolutions are unprecedentedly high as meteor wind measurements [Tsutsumi et al., JPGU 2023].

This technique is now being applied to MF radars at the northern hemisphere, Saura (69N, 16E) and Juliusruh (54N, 13E), routinely operated by Leibniz Institute of Atmospheric Physics. These radars are well equipped with an interferometer capability with 9 and 6 receiver channels, respectively. We have found that existing archived data of these radar systems can be applicable to the meteor echo analyses as those we have done with the Syowa system.

However, one radar measurement can provide only radial wind component, not the tangential component. This means that the vorticity is hard to estimate with one radar system, hindering further statistical analyses of the wind field.

To overcome this limitation we are now trying to conduct common volume meteor measurements using two MF radar systems in the northern high latitude, that is, the Saura system mentioned above and the Tromsoe system (70N, 19E) operated by Arctic University of Norway. Because the Tromsoe system has currently only limited number of receiving antennas and channels, we are planning to add a digital receiver and antenna system to enable all-sky interferometer measurements. The Saura and Tromsoe systems are ideally separated to share a common illuminating volume, and are expected to resolve fine time and spatial structures of wind fields, even with much better resolutions than those of recent VHF meteor radar based network measurements.

References

Tsutsumi, M. and Aso, T. MF radar observations of meteors and meteor-derived winds at Syowa (69S, 39E), Antarctica: A comparison with simultaneous spaced antenna winds, Journal of Geophyiscal Research-Atmospheres, 110, doi:10.1029/2005JD005849, 2005.

Tsutsumi, M., Renkwitz, T., and Chau, J. L., High resolution wind observations based on MF radar meteor echo measurements in the northern and southern mid-to-high latitudes, Japanese Geoscience Union Meeting, Makuhari, May 2023.

Incoherent scatter and coherent scatter echoes from the ionosphere observed by the PANSY radar

A. Saito[1], D. Kagawa[2], T. Hashimoto[3], and K. Nishimura[4]
[1]*Graduate School of Science, Kyoto University, JAPAN*
[2]*Mitsubishi Electric Corporation, JAPAN*
[3]*National Institute of Polar Research, JAPAN*
[4]*Research Institute for Sustainable Humanosphere, Kyoto University, JAPAN*

Program of the Antarctic Syowa MST/IS radar (PANSY radar) is a large VHF atmospheric radar located at Syowa Station, Antarctica. PANSY can detect the incoherent scatter (IS) echoes from the ionospheric electron between 100km and 500km altitude. The amplitude of the IS echoes is proportional to the electron density, and the altitude profiles of the ionospheric electron density can be derived from the IS echoes. The echo intensity is calibrated with the ionosonde data at Syowa station. The ion velocity and ionospheric temperature can be observed with multi-pulse IS observation, too. Besides the IS echoes, coherent echoes from the ionosphere are also detected by the PANSY radar. Coherent echoes are mainly scattered by the ionospheric field-aligned irregularities (FAIs) whose wavelength is half of the wavelength of the radar radio wave. FAIs stretch along the geomagnetic field lines. The amplitude of the coherent echoes from FAIs is related to the ionospheric instabilities generating FAIs. These two types of echoes are utilized to elucidate the ionospheric phenomena over the Syowa station. PANSY detects these two echoes simultaneously. For the IS observations, coherent echoes are a source of contamination and should be removed. Hashimoto et al. (2019) developed an adaptive signal-processing technique to suppress the coherent echoes to derive clear IS echoes. IS observation to observe the ionospheric electron density structures has been carried out regularly in 2024. On the other side, FAIs have also been studied because the FAI structures are related with the auroral precipitations and the electric current that causes the instabilities. An effective imaging method has been developed to capture the FAI structures in the field of view of PANSY. Two sub-arrays of PANSY, the FAI array, and the meteor array, are used in this FAI imaging method. The outline of PANSY radar's ionospheric observation of incoherent scatter and coherent scatter echoes will be introduced and discussed in the presentation.

References

Hashimoto, T., A. Saito, K. Nishimura, M. Tsutsumi, K. Sato, and T. Sato (2019), First incoherent scatter measurements and adaptive suppression of field-aligned irregularities by the pansy radar at syowa station, antarctic. Journal of Atmospheric and Oceanic Technology, 36, 9, 1881–1888, https://doi.org/10.1175/JTECH-D-18-0175.1.

Variations in the ozone concentration in the mesosphere observed at Syowa station associated with energetic particles precipitation

Hikaru Suzuki[1], Fuminori Tsuchiya[1], Ryo Mizuno[2], Isao Murata[1], Yasumasa Kasaba[1], Tomoo Nagahama[2], and Hirofumi Goto[2]

[1]*Tohoku university*

[2]*ISEE, Nagoya university*

We report variations in ozone concentration in the mesosphere above Syowa station, Antarctica, caused by energetic particle precipitation (EPP) associated with a major magnetic storm that occurred from May 10th to 11th, 2024. The goal of this study is to clarify the decrease in O3 concentration in the mesosphere associated with EPP during night.

In polar regions, EPP are associated with solar proton events and magnetic storms. The higher the energy of these particles, the lower the altitude of the precipitate. If an electron has an energy of approximately 300 keV or higher, it precipitates at an altitude below 70 km. The ionization of atmospheric molecules induced by the EPP produces nitrogen oxide(NOx) and hydrogen oxide in the mesosphere, which could cause O3 destruction. In addition to the direct effect of EPP, EPP may have an indirect effect on O_3 in the lower atmosphere through the transport effects. NOx produced in the lower thermosphere can reach the upper stratosphere via polar winter descent, where it can participate in catalytic reactions that destroy O_3. Since O_3 is a significant component distributed across a wide range of altitudes and has a crucial impact on climate, it is necessary to investigate the effects of EPP.

We used a millimeter-wave spectroradiometer installed by Nagoya University at Syowa station in Antarctica. Long-term observations of the spectral lines of nitric oxide (NO) and O_3 began in 2012. In 2022, simultaneous observations of two O3 emission lines in the 250 GHz band carbon monoxide (CO) emission lines in the 230 GHz band, and six NO emission lines in the 250 GHz band were started. The spectrum observed by the millimeter-wave spectroradiometer on the ground is an integration of the O3 radiation over altitudes from the surface to the lower thermosphere. We retrieved the altitude distribution of the O3 volume mixing ratio (VMR) from the radiation spectra to quantitatively estimate the O3 concentration in the mesosphere. The observed spectra used for the retrieval are integrated over one hour. When the optical depth varies significantly with time due to weather conditions, the data are excluded from the analysis. Thus, up to 24 O_3VMR profile data are obtained per hour per observation day. The retrieval tool uses the O3 height distribution obtained by the MLS satellite as an a-priori distribution and estimates the vertical distribution of O3VMR from the model spectrum that best matches the observed spectrum, using the NASA-JPL molecular spectroscopy catalog and the meteorological vertical profile data from MERRA2. Since the altitude distribution of O3 is affected by sunlight, a-priori distributions for daytime and nighttime are switched at times of sunset and sunrise.

We have analyzed the data from May 1st to 23rd. From May 10th to 11th, an increase in the flux of protons with energies above 100 MeV was confirmed from GOES satellite data. No clear increase was observed in the EPP flux data over Syowa station from the POES satellite. The riometer installed at Syowa station confirmed an increase in precipitating electrons between 17:00 UT and 18:30 UT on May 10th. We found a decrease in the mesospheric (60–70 km) O_3 column amount during the night from May 10th to 11th. The decrease in the average O_3 column amount during that night with the previous night was approximately 0.035 D.U., which represents the largest change in the daily mesospheric O_3 column amount during the analysis period. When examining the hourly changes in the mesospheric O_3 concentration profiles from 15:00 on May 10th (LT18:00 at Syowa station) to 3:00 on May 11th (LT6:00), a decrease was observed from around LT19:00 to LT22:00. This was followed by an increase LT22:00 to LT23:00 and another decrease from LT23:00 to LT06:00. This pattern differs from the typical diurnal variation in O_3 column amounts. In addition to the major magnetic storm from May 10th to 11th, moderate magnetic storms ranging from -50 to -100 nT occurred in May 2024, leading to increased proton and electron precipitation. In this presentation, we will report variations in the O_3 concentration in the mesosphere over Syowa station associated with EPP during May 2024.

Large amplitude perturbations in equatorward wind surges during the intense geomagnetic storm on 3-4 November 2021

Jonna Wehmeyer[1], Yoshihiro Tomikawa[1,2], Takanori Nishiyama[1,2]
1. The Graduate University for Advanced Studies, 2. National Institute of Polar Research

During geomagnetic storms energy is injected into the high latitude atmosphere via precipitating particles and strong electric fields that map down from the magnetosphere to the ionosphere. The acceleration of the ionospheric plasma leads to joule heating of the thermosphere producing a steep latitudinal pressure gradient. The resulting strong equatorward winds are important to the middle and low latitude ionospheric response to magnetic storms by driving the ionospheric disturbance dynamo whose effects last on even after the high latitude ionosphere already recovered [Blanc and Richmond, 1980]. Disturbances of those equatorward winds might have a significant impact on the evolution of the disturbance dynamo, but scale and occurrence rate of strong disturbances are poorly understood [e.g. Shiokawa et al., 2003; Zhang et al., 2015; Guo et al., 2018]. In this study we searched for variations in the equatorward surge at mid-latitudes and especially focused on disturbances at which the thermospheric wind reverses and turns northward.

To investigate thermospheric winds we used data from ICON MIGHTI observations, and data from FPIs distributed over north and middle America. For ICON MIGHTI observations we focused on simultaneous observations with FPIs characterized by a radial distance of less than 500 km at 250 km altitude, which is the approximate altitude of red line (630.0 nm) observations made by both instruments. ICON MIGHTI observations are limb observations, which means that the observed winds are integrated over a horizontal line of sight, which makes it difficult to identify local perturbations. Simultaneous observations enable us to combine information about averaged background winds with information about local wind changes, so we can gain a more holistic image of local conditions at FPI observatories. To search for travelling ionospheric disturbances that originate from thermospheric winds we used the GNSS TEC data binned 1 degree longitude by 1 degree latitude at a 5-minute interval.

This poster focuses on a strong geomagnetic event from November 3rd to November 4th, 2021, with a peak Kp index of 8^{-} and a SYM-H low-peak of -118nT on November 4th. The strong storm was preceded by several moderate geomagnetic disturbances beginning on October 27th [Geleta and Mengistu Tsidu, 2024]. Previous studies have analyzed the intensity and effect of the storm induced equatorward surge with wind speeds up to 250 m/s [e.g. Regi et al., 2022; Gan et al., 2024], but FPI observations also show significant perturbations, some with rapid changes in wind speed of over 300 m/s. In this poster we present a detailed analysis of the characteristics of such disturbances.

OSp10

Study of long-term ionospheric variations based on Tromsø Ionosonde and EISCAT radar data

Y. Ogawa[1], M. G. Johnsen[2], N. Gulbrandsen[2], A. Løkke[2], I. Mann[3], and I. Häggström[4]
[1]*National Institute of Polar Research, Japan*
[2]*Tromsø Geophysical Observatory, UiT the Arctic University of Norway, Norway*
[3]*Department of Physics and Technology, UiT the Arctic University of Norway, Norway*
[4]*EISCAT Headquarters, Sweden*

We have studied long-term ionospheric variations using a combination of data from the Tromsø Ionosonde since 1932 and the EISCAT Tromsø UHF radar since 1981. To investigate Arctic ionospheric variations in connection with the Arctic warming and cooling before 1970s, we have developed a Tromsø ionosonde database capable of analyzing daily variations over about 90 years. During the 1940s~1960s, when cooling was occurring on the Arctic surface, a clear increasing trend in *foF2* were seen in the Tromsø ionosonde data: a rate of 0.32 ± 0.10 [MHz/decade]. It can be explained by the energy balance of the entire Earth's atmosphere. As for the trend of foF2 since 1994, there has been a gradual decline, at a rate of -0.13 ± 0.05 [MHz/decade].

A unified database for 43 years, from 1981 to 2023, has been created from the EISCAT Tromsø UHF radar. The analysis of 43 years of data show that clearer ion temperature decreases at an altitude of 300 km at a rate of 1.6 ± 0.2 [K/year], compared to the previous analysis using 33-year EISCAT data (Ogawa et al., 2014). A detailed comparison of the ionosonde data with the EISCAT radar data will allows us to understand how various ionosonde parameters are related to ionospheric plasma parameters such as ion/electron density and temperature. By applying the results to the early ionosonde data, it will provide clues to understanding how the Arctic warming and cooling before 1970s affected the upper atmosphere in the Arctic region.

References

Ogawa, Y., T. Motoba, S. C. Buchert, I. Häggström, and S. Nozawa, Upper atmosphere cooling over the past 33 years, *Geophys. Res. Lett*., 41, 5629-5635, doi:10.1002/2014GL060591, 2014.

Feasibility study to estimate the ion velocity field in the *F*-region from EISCAT_3D radar observations

Mizuki Fukizawa[1], Yasunobu Ogawa[1], Genta Ueno[2], Koji Nishimura[3], Takanori Nishiyama[1], Taishi Hashimoto[1], Takuo Tsuda[4]

[1]*National Institute of Polar Research*

[2]*The Institute of Statistical Mathematics*

[3]*Kyoto University*

[4]*University of Electro-Communications*

In the ionospheric *F*-region, both the ions and electrons drift in the ExB direction. For example, sheared flow is often observed as associated with an aurora arc, and high-speed flow is caused in the subauroral region, which is called subauroral polarization streams. Therefore, the electric field distribution is important to understand the electrodynamics in the ionosphere and the magnetosphere-ionosphere coupling process because the electric field distribution affects the electric current system. The electric and ion velocity fields can be estimated from the line-of-sight (LOS) ion velocity observed by incoherent scatter radars. Several reconstruction methods have been proposed, but these methods were customised for each radar because the direction and number of beams depend on the observation target and radar location. This study aims to estimate the ion velocity and electric fields in the *F*-region, considering the beam configuration for Common Programme observations for the EISCAT_3D radar.

The reconstruction was conducted by maximizing a posterior probability based on Bayes' theorem. To solve the underdetermined problem, we gave the constraint which minimizes the L2 norms of the second derivative of three components of the ion velocity vector. There are nine terms to calculate the second-order derivatives in the three directions x, y and xy for the three velocity components, with nine coefficients set as weights for each term. The hyperparameters were determined by finding a maximum value of the marginal likelihood using the grid search method. A synthetic flow field was prepared to validate the reconstruction method. LOS velocity was observed by 27 beams from 3 stations. Uncertainty of LOS velocity was calculated using "E3Doubt" with the transmitter power of 3.5 MW and the integration time of 2 s per beam. It was assumed that ions move with the same E × B drift velocity at 200–500 km altitudes to increase observation data. Observation noise was reduced by averaging the data within each grid.

We have performed reconstructions for three synthetic velocity fields and validated their accuracy: 1) east-west sheared flow, 2) northeast-southwest sheared flow, and 3) undulating sheared flow. The reconstruction accuracy was evaluated by calculating the relative residual as follows: relative residual [%] = (estimated field - true field) / (true field) × 100. The reconstruction accuracy was high for east-west sheared flow with a relative residual of 12–16% on ~90% grids. On the other hand, the relative residuals were larger when the sheared flow field was tilted or undulated, ranging from 0-35% on a ~85% grid. Although the relative residuals were larger near the edges where there was no observational data, the direction of flow fields was well reconstructed. The divergence of the electric field, which is required to derive the field-aligned current, was reconstructed with an accuracy of 12% for Case 1, while that for Cases 2 and 3 were underestimated up to 100%. A possible reason for the low accuracy of the reconstruction of tilted and undulating velocity fields is that the nine hyperparameters are not well determined. In the current analysis, the hyperparameters were determined by maximising the marginal likelihood by grid search. However, due to a large number of parameters, the number of parameters to be changed is limited to three, and the search for the maximum value was carried out by changing the parameters to be varied in turn. It is necessary to consider a method that can search for the maximum value more accurately.

Over-darkening of diffuse/pulsating aurora: LAMP sounding rocket observation

T. Noda [1], Y. Miyoshi[1], K.Hosokawa[2], K,Asamura[3], T.Sakanoi[4], M.Lessard[5], A. Jaynes[6], M.Shumko[7], A.Halford[8], T. Namekawa[9], T. Mitani[3], M. Nose[10], M. McHarg[11], V. Ledvina[12] and D. Hampton[12]

[1]ISEE, Nagoya University
[2]University of Electro-Communications, Tokyo, Japan
[3]Institute of Space and Astronautical Science, JAXA, Sagamihara, Japan
[4]Tohoku University, Sendai, Japan
[5]University of New Hampshire, Durham, US
[6]University of Iowa, Iowa, US
[7]Applied Physics Laboratory, Johns Hopkins University, Maryland, US
8. Goddard Space Flight Center, NASA, Maryland, US
9. National Institute of Information and Communication Technology, Tokyo, Japan
10. Nagoya City University, Nagoya, Japan
11. The United States Air Force Academy, Colorado, US
12. University of Alaska, Fairbanks, US

Pulsating aurora is a kind of diffuse aurora that modulates their luminosity with a period ranging from a few to 10 seconds. The over-darkening, in which the brightness is decreased by several tens of percent against background, has been observed just after the luminosity enhancement during the pulsation “ON” time. There have been various reports on over-darkening after pulsating auroras, but details about the over-darkening have not yet been revealed. We have studied the over-darkening phenomena associated with the pulsating aurora using the observation data of electron observations (EPLAS) and optical observations (AIC) onboard the LAMP sounding-rocket experiments, which was launched on March 5, 2022 at Poker Flat Research Range. EPLAS can observe electrons in the 10eV-20keV energy range, and AIC can observe optical emissions in the 667-680nm and 844-848nm wavelength ranges. An event of the over-darkening is observed during the flight operation of the LAMP sounding rocket. The optical aurora emission at the footprint of the LAMP rocket observed by AIC decreased from 3,000 Rayleigh to 1,300 Rayleigh, and the downward energy flux observed from EPLAS dropped by ~50%. The energy flux significantly decreases above 5 keV, especially the flux at 6.6 keV decreased ~40%. Considering the resonance condition with whistler mode chorus waves, the attenuation of precipitation at high-energy electros is caused by a decrease of the pitch angle scattering with the chorus waves. In the presentation, we will show detail variations of energy spectrum and pitch angle distribution of precipitating electrons during the over-darkening and discuss possible mechanisms.

OSp13

Investigation of Omega Band Auroras: Ground and Magnetospheric Conjugate Observations

I.Naganawa[1], Y. Miyoshi[1], S. Kurita[2], K. Hosokawa[3], S. Oyama[1], Y. Ogawa[4], Y. Kasahara[5], S. Matsuda[5], T. Hori[1], Y. Kazama[6], S.-Y. Wang[6], C.-W. Jun[1], S. Kasahara[7], S. Yokota[8], K. Keika[7], A. Matsuoka[2], M. Teramoto[9], K. Yamamoto[1], and I. Shinohara[10]

[1] *ISEE, Nagoya University*

[2] *Kyoto University*

[3] *The University of Electro-Communications*

[4] *National Institute of Polar Research*

[5] *Kanazawa University*

[6] *ASIAA, Taiwan*

[7] *University of Tokyo*

[8] *Osaka University*

[9] *Kyushu Institute of Technology*

[10] *iSAS/JAXA*

The Omega band auroras are a type of aurora that occur after auroral breakups, characterized by a structure resembling an inverted Greek letter Omega (Ω). These auroras drift eastward from midnight towards dawn.
Several theories have been proposed to explain the origin of Omega band auroras, including a model suggesting their formation due to velocity shear induced by a hybrid of Kelvin-Helmholtz and Rayleigh-Taylor instabilities. Another model proposes that polar auroral streamers evolve directly into the torch structures of Omega bands. Also it has also been revealed that Omega band auroras are composed of various types of auroras, including diffuse, pulsating, and discrete auroras within the torch structures. However, the magnetospheric mechanisms responsible for Omega band auroras remain unclear due to a lack of simultaneous observations from magnetospheric satellites.
In this study, we analyzed ground-based observations at two wavelengths (427.8 nm and 844.6 nm), using two EMCCD cameras installed in Tromsø, Norway, along with conjugate observations by the Arase satellite on the magnetospheric side. On September 30, 2019, and March 25, 2021, Omega band auroras were observed in Tromsø, with the Arase satellite's orbital footprint within the field of view of the optical camera. These events occurred during dawn local time. During these events, the Arase satellite detected injections of tens of keV electrons along with strong chorus waves, which could be the origin of the diffuse and pulsating auroras observed within the Omega band auroras.
In this presentation, we will report on the spatial characteristics of precipitating electrons within the Omega band auroras and their correspondence with magnetospheric phenomena observed during these two events.

Investigation of more efficient and faster auroral 3D reconstruction

Yoshimasa Tanaka[1,2,3], Yasunobu Ogawa[1,2,3], Mizuki Fukizawa[2], Keisuke Hosokawa[4], and Akiko Fujimoto[5]

[1] *Polar Environment Data Science Center, Joint Support-Center for Data Science Research, Research Organization of Information and Systems*
[2] *National Institute of Polar Research*
[3] *The Graduate University for Advanced Studies (SOKENDAI)*
[4] *The University of Electro-Communications*
[5] *Kyushu Institute of Technology*

We have developed the generalized-auroral computed tomography (G-ACT) method, which is able to reconstruct three-dimensional (3D) distribution of auroral emission from multi-instrument data, such as monochromatic images taken at multi-point imager network and ionospheric electron density from radars (Tanaka et al., 2011). We believe that this method will be useful for auroral 3D research especially when combining multiple auroral images with the electron density data obtained by the EISCAT_3D radar (Tanaka et al., 2024), which is planned to be operated in the near future. However, the auroral 3D reconstruction has been limited to a small number of case studies so far because it takes a long time to process data, solve the inverse problem, and visualize the 3D reconstruction results, in addition to a lack of data suitable for auroral tomography analysis. In this study, therefore, we investigate how to improve the auroral 3D reconstruction more efficient and faster. One possibility is the use of simulation with modeled auroral images for G-ACT. One of the most time-consuming process in G-ACT is to determine hyper-parameters that are associated with the weights between different data types and the regularization. The optimal hyper-parameter values cannot be fixed and need to be tuned according to observation conditions such as auroral shape, imagers' location, and signal to noise ratio. Thus, we pre-calculate hyper-parameters under various conditions using model simulations and compile them into a database to automatically determine the appropriate hyper-parameters for the observed data. The simulation also enables us to estimate errors in the analysis results. The other challenge is to apply the state-of-the-art 3D reconstruction and visualization methods using the machine learning or deep learning technique. We discuss the feasibility of these attempts at more efficient and faster auroral 3D reconstruction.

References

Tanaka, Y.-M., T. Aso, B. Gustavsson, K. Tanabe, Y. Ogawa, A. Kadokura, H. Miyaoka, T. Sergienko, U. Brändström, and I. Sandahl, Feasibility study on Generalized - Aurora Computed Tomography, Annales Geophysicae, 29(3), 551–562, doi:10.5194/angeo-29-551-2011, 2011.

Tanaka, Y.-M., Y. Ogawa, A. Kadokura, T. Aso, B. Gustavsson, U. Brändström, T. Sergienko, G. Ueno, S. Saita, Application of Generalized - Aurora Computed Tomography to the EISCAT_3D project, Ann. Geophys., 42, 1, 179-190, https://doi.org/10.5194/angeo-42-179-2024, 2024.

New multi-wavelength all-sky imager systems for observation of polar cap aurora

*Takeshi Sakanoi[1], Ryuho Kataoka[2], Aya Otomo[1], Yoshimasa Tanaka[2]
Keisuke Hosokawa[3], Yuta Hozumi[4], Shin-ichiro Oyama[5], Satoshi Ishii[6], Kiyoka Murase[2], Yusuke Ebihara[7]
[1]*Planetary Plasma and Atmospheric Research Center, Graduate School of Science, Tohoku University*
[2]*National Institute of Polar Research,* [3]*The University of Electro-Communications,* [4]*Catholic University of America*
[5]*ISEE, Nagoya University,* [6]*Rikkyo University,*[7] *Kyoto University*

We report a multi-wavelength all-sky imager system, and give a summary of observation results and future plans. Since auroral emission happens at a certain altitude depending on the precipitating electron energy, simultaneous multi-wavelength auroral imaging are important to understand the coupling processes between magnetosphere, ionosphere and middle atmosphere. We originally developed the multi-wavelength all-sky imaging system which consists of two compact CMOS cameras with bandpass filters on the Antarctic icebreaker Shirase in 2019 (the Shirase system). This system was installed on the gimbal that canceled the oscillations of Shirase during the cruise between Japan and Syowa Station, and had the capability to carry out automatic continuous observations during the nights. Although the system is stable and useful for automatic operation, the fastest interval between two exposures is limited to ~2s.

On the other hand, we developed another observation system for the auroral camera AIC on the LAMP rocket which was launched successfully in 2022 (the LAMP system). The observation system was applied to the ground auroral imagers on Arctic stations. This system is characterized for high-speed imaging with an interval up to ~20 frame/sec.

Taking advantages of the Shirase system and LAMP system, we developed the all-sky imager systems mainly for the phase X Priority Research program of the NIPR. The period of phase-X (FY2022-2027) involves the solar maximum, and we expect to obtain sufficient data at high-latitude Antarctic region. The polar cap region is particularly important since the direct interaction between the solar wind and atmosphere happened in by precipitating electrons and ions in a wide energy range from hundreds eV (typical solar wind) to MeV (SEP). SEP causes the ionization in the middle atmosphere and induce chemical processes including O3, HOx, and NOx, and may change temperature structure.

The all-sky camera system consists of CMOS sensor (ZWO ASI183MM Pro or ASI183MM), fisheye lens (Fujinon FE185C086HA, f=2.7 mm, F/1.8), and Andover interference filter. The filter is equipped between the lens and sensor to minimize the whole optical system and bring us a monochromatic image. The cameras are controlled by mini-PCs (ESC LIVA-Q2, OS: Linux Ubuntu). The data are stored on a NAS (Synology) with a mode of RAID-1 (mirroring) via network. The LIVA PCs, NAS and router are powered by an internet switch (Watchboot). Watchboot is capable of ping monitoring via the internet, and when there is no response from the PC and so on, power turns off and on to recover.

We summarize the past observations, current status of the operation and future plan of the all-sky imager systems in Table 1. We installed the system at the Syowa Station as a part of JARE 64. and started continuous operation since the Antarctic winter of 2023. The wavelengths are N2+ 391.4 nm, O 557.7 nm, O 630.0 nm, N2 670.0 nm. The exposure time for the cameras of 391.4 nm and 630.0 nm is 18 sec with a cadence of 20 sec, and that for the cameras of 557.7 nm, 670.0 nm is sampled with up to ~10 frame/sec.

In addition, we installed the three auroral cameras at the Skibton Station, Norway in this August. The main purpose of this observation is to check the functions and observation data qualities which will be taken by the new AIC camera on the LAMP-2 rocket. Therefore, two cameras out of three cameras are controlled by the LAMP system and one is by the Shirase system. In addition, as shown in Table 1, we developed four all-sky cameras for the Casey and Davis Stations. Furthermore, we are currently developing four all-sky cameras for the Dumont d'Urville and Dome-C stations. These cameras will be transported to these Antarctic stations in 2024, and scheduled to start the automatic operation in 2025. We also plan to install similar camera system at the South Pole of which data provide us key data for the scientific objectives of the Antarctic phase X program.

Table 1. Station, wavelength and operation period of the all-sky imager system.

Station	Wavelength(nm)	Operation Period
Shirase	630, 670, 760	2019 - 2022
Syowa	391.4, 557.7, 630, 670	2023 -
KHO, Svalvard	391.4, 630	2022 - 2023
Skibton	670, 844.6	2024 -
Casey	391.4, 630	2025 -
Davis	391.4, 630	2025 -
Dumont d'Urville	391.4, 630	2025 -
Dome C	391.4, 630	2025 -
South Pole	391.4, 486, 557.7, 630, 670, 844.6	TBD

Geometric Structure of Magnetic Fields in Earth's Magnetosphere: The Role of the Hall Effect*

Ryuji Shimokawa[1], Akimasa Yoshikawa[2]

[1] *Department of Earth and Planetary Sciences, Graduate School of Science, Kyushu University.*
[2] *Department of Earth and Planetary Sciences, Faculty of Sciences, Kyushu University.*

Understanding the response of magnetospheric convection to magnetic field variations is crucial in magnetospheric physics. Among the fundamental processes governing this response, magnetic reconnection spans a wide range of scales, from microscopic to macroscopic. In the context of hydrodynamics, during magnetic reconnection, electrons follow magnetic field lines into the diffusion region, while ions remain at a distance defined by the ion inertial length. This differential motion generates a Hall current. Nagai et al. (1998), using Geotail satellite data, were the first to observe the decoupling of ions and electrons near the reconnection site. More recently, the Magnetospheric Multiscale Mission (MMS; Burch et al., 2016), with spacecraft separations ranging from several ion inertial lengths to electron inertial lengths, has provided detailed observations of structures at both ion and electron scales within Flux Transfer Events (FTEs; e.g., Russell & Elphic, 1978). Recent studies, such as Hawing et al. (2021), have demonstrated that microscale (electron) and mesoscale (ion) processes in the vicinity of FTEs are critical for their formation, structure, and evolution.

In both magnetic reconnection and in the microscale and mesoscale processes surrounding FTEs, the Hall effect plays a key role in the evolution of the magnetic field and associated plasma motion. In Hall-MHD, the magnetic field's time evolution is governed not only by plasma motion perpendicular to the magnetic field, as in ideal MHD, but also by an induced electric field proportional to the Ampère force (J×B). The Ampère force, which serves as the primary driver of plasma acceleration, becomes particularly prominent in the reconnection region, significantly influencing the induced magnetic field. Furthermore, the development of a generalized magnetic field coordinate system, evolving dynamically in space and time with plasma dynamics, allows for a more precise description of complex three-dimensional magnetic field structures (Yoshikawa, 2020).

In this study, we applied the geometric analysis framework of magnetic field evolution developed by Yoshikawa (2020) to Hall-MHD, aiming to examine the geometric effects of magnetic field dynamics. Our findings elucidate the topological changes in the magnetic field due to magnetic field generation driven by the rotation of magnetic tension and provide a geometric interpretation of the generation of the Hall quadrupole field, which enhances the perpendicular magnetic field—a hallmark of the Hall effect. Building on the simulation results of Hawing et al. (2021), we propose new approaches for describing the local structures within magnetic reconnection and the topological changes occurring during the kinetic processes inside FTEs. Additionally, we discuss how the micro- to mesoscale dynamics within FTEs can influence their macroscale properties.

****References****

Nagai, T., Fujimoto, M., Saito, Y., Machida, S., Terasawa, T., Nakamura, R., Yamamoto, T., Mukai, T., Nishida, A., & Kokubun, S. (1998). Structure and dynamics of magnetic reconnection during substorm onsets observed by Geotail. *Journal of Geophysical Research: Space Physics*, 103, 4419–4440. https://doi.org/10.1029/97JA02190

Hwang, K.-J., Burch, J. L., Russell, C. T., Choi, E., Dokgo, K., et al. (2021). Kinetic structure and dynamics of ion-scale flux transfer events observed by MMS. *The Astrophysical Journal*, 914(1), 26. https://doi.org/10.3847/1538-4357/abf8b1

Formation of lobe and plasma sheet in the northward IMF condition based on the fundamental mechanical principle

Shigeru Fujita[1,2] Takashi Tanaka[3], Masakazu Watanabe[4,3], and DongSheng Cai[5]

[1] *Joint Support-Center for Data Science Research, ROIS*

[2] *The Institute of Statistical Mathematics, ROIS*

[3] *International Research Center for Space and Planetary Environmental Science, Kyushu University*

[4] *Department of Earth and Planetary Sciences, Faculty of Science, Kyushu University*

[5] *Graduate School of Science and Technology, University of Tsukuba*

The solar wind and the magnetosphere are both composed of magnetohydrodynamic (MHD) fluids, and they are treated as a single system. The vacuum magnetic field, which appears when plasma is removed from this system and has no free energy, represents the ground state of the system. Therefore, the physical processes of this system follow the mechanical principle where the deforming force exerted by the plasma on the magnetic field is balanced by the restoring force of the magnetic field (the mechanical principle). Additionally, the vacuum magnetic field contains null points of the magnetic field, inherently providing a site for magnetic reconnection. Furthermore, in the case of a northward interplanetary magnetic field (IMF), the magnetic field deformed by the solar wind also retains the topology of the vacuum magnetic field (the topology conservation property). The purpose of this study is to establish the fundamental physical processes of the solar wind-magnetosphere system, considering it as a unified system based on the mechanical principle that takes into account the topology conservation property. This study mainly presents an understanding of the magnetospheric structure and its dependence on solar wind parameters under fundamental principles, particularly under northward IMF conditions. In the talk, we will present the physical processes of the formation of the lobe and the plasma sheet based on the fundamental principles.

Origin of the nightside ionospheric convection for interplanetary magnetic field conditions of $B_z >> |B_y| > 0$: An extremely modified Dungey cycle concurrent with the interchange cycle

Watanabe Masakazu[1], Cai DongSheng[2], Xiong Peikun[2], Fujita Shigeru[3] and Tanaka Takashi[4]
[1]*Graduate School of Science, Kyushu University*
[2]*Institute of System and Information, University of Tsukuba*
[3]*Joint-support center for data science research, The Institute of Statistical Mathematics*
[4] *International Research Center for Space and Planetary Environmental Science, Kyushu University*

When the interplanetary magnetic field (IMF) is southward, the geomagnetic field lines on the dayside magnetopause transmute from closed to open and transported tailward. They become closed again in the magnetotail and transported sunward to finally return to the dayside, thus forming a magnetic flux circulation called the Dungey cycle (Dungey, 1961). The two reconnection processes associated with the Dungey cycle are both called Dungey-type. Topologically, in Dungey-type reconnection, four distinct regions meet together on a separator. In contrast, when the IMF is close to due north, another magnetic flux circulation called the interchange cycle is formed (Watanabe and Sofko, 2009). The interchange cycle is characterized by a pair of "reverse" convection cells on the dayside ionosphere whose circulation directions are opposite to those driven by the Dungey cycle. The name "interchange" comes from the fact that the magnetic flux circulation consists of two interchange-type reconnection processes (i.e., IMF-to-lobe reconnection and lobe-to-closed reconnection). The interchange-type reconnection is a process in which two topological regions meet together on a separatrix excluding the separators. Although the Dungey cycle for southward IMF and the interchange cycle for northward IMF appear to be mutually exclusive, they can coexist. One example is the IMF B_y-dependent ionospheric convection that appears occasionally on the nightside when the IMF is northward (Grocott et al., 2005). Recently, using a global magnetohydrodynamic (MHD) simulation, Tanaka et al. (2024) interpreted this convection system as a manifestation of the partial Dungey cycle that is concurrent with the dayside twin reverse cells associated with the interchange cycle. The purpose of this study is to explain the seemingly-strange concurrence of the two opposing magnetic flux circulation cycles from a topological point of view. From MHD simulations, we reproduced the IMF B_y-dependent convection system on the nightside and investigated how the two magnetic flux circulations can coexist. The magnetic topology of the magnetosphere for northward IMF consists of two magnetic nulls and two separators connecting them. When the IMF is close to due north, the two separators bend sharply in the vicinity of the magnetic nulls. This bend enables both types of reconnection to coexist in the neighborhood of the null point. However, the geometry of Dungey-type reconnection is quite different from that for southward IMF. In the presentation, we discuss the separator configuration in detail that allows the concurrence of the two magnetic flux circulations.

References

Dungey, J. W. (1961). Interplanetary magnetic field and the auroral zones. Physical Review Letters, 6, 47–48. https://doi.org/10.1103/PhysRevLett.6.47

Watanabe, M., and Sofko, G. J. (2009). The interchange cycle: A fundamental mode of magnetic flux circulation for northward interplanetary magnetic field. Geophysical Research Letters, 36, L03107. https://doi.org/10.1029/2008GL036682

Grocott, A., et al. (2005). Interhemispheric observations of the ionospheric signature of tail reconnection during IMF-northward non-substorm intervals. Annales Geophysicae, 23, 1763–1770. https://doi.org/10.5194/angeo-23-1763-2005

Tanaka, T., et al. (2024). Multiple convection cells induced by in-front and off-front interactions between the obliquely northward IMF and the geomagnetic field. Journal of Geophysical Research: Space Physics, 129, e2023JA031994. https://doi.org/10.1029/2023JA031994

Progress report on the imaging receiver system at the SuperDARN Hokkaido East radar (2024)

Nozomu Nishitani[1], Yoshiyuki Hamaguchi[1], Tomoaki Hori[1], and Shota Hayamizu[1]
[1]*Institute for Space-Earth Environmental Research, Nagoya University*

The Super Dural Auroral Radar Network (SuperDARN) is a network of high-frequency (HF) radars deployed to monitor ionospheric dynamics. More than 35 SuperDARN radars are deployed in both hemispheres, covering the polar cap, aurora, sub-aurora, and mid-latitude regions.

A typical SuperDARN operating mode is the normal scan program, which scans the entire radar field of view every 1 to 2 minutes. Conventional SuperDARN radars typically have a single receive channel (scanning one beam direction at one time). Therefore, the typical Nyquist frequency for conventional normal scan SuperDARN radar data is 4 to 8 mHz. This time resolution is not suitable for dealing with short term variations such as Pi2 / Pc3 pulsations or space ionospheric disturbances.

During the previous symposiums on Polar Science in 2021 and 2023, plans were presented to implement an image receiver system on one of the mid-latitude SuperDARN radars, the SuperDARN Hokkaido East Radar. In this presentation, we show the latest progress report on this system. This system utilizes the USRP SDR unit used in the remote receiver for the SuperDARN Hokkaido East radar signal in Nagoya (Nishitani et al., 2021). We have already manufactured a 4-channel subset prototype system (of the 20-channel system) and successfully tested it at a radar site in July 2020. We have developed a 20-channel, full-specification system, which is being tested at a laboratory at ISEE, and will be sent to the radar site after the system is complete. Figure 1 shows the device currently under testing. We are nearing the end of the calibration of the receiver hardware and will be working on building a data storage system that will need to store vast amounts of data in real-time.

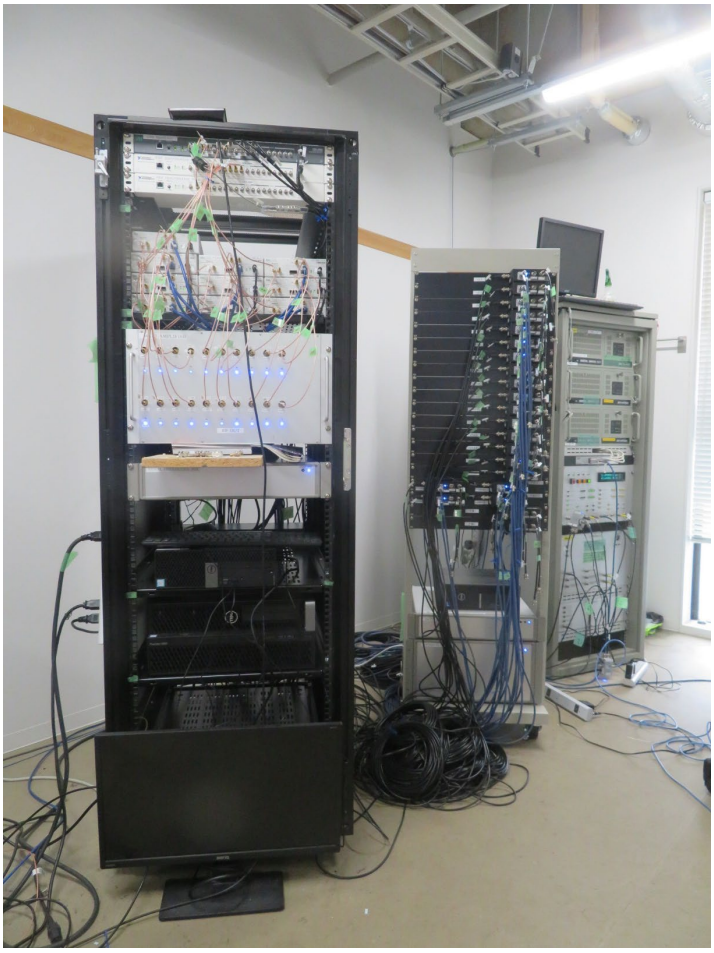

Figure 1. Photo of the main amplifier and control units for the 20-channel imaging receiver system (front), and the head-amplifier (middle). They are now under now under development and to be installed at the SuperDARN Hokkaido East radar site.

The new image receiver system is expected to be able to acquire data with temporal and spatial resolution several times higher than the existing systems. With the new system we expect to deal with the following topics: (a) Study of a variety of scientific phenomena, such as ULF waves (e.g. Pi2 / Pc3) with periods shorter than 1 minute. (b) Transients excited by external (IMF / solar wind) and internal (e.g. onset of substorm expansion) environmental changes in the ionosphere and magnetosphere. (c) Ionospheric disturbances caused by sudden changes in the earth's surface, such as earthquakes and volcanic eruptions. More details on the latest progress report on the Imaging receiver system will be presented.

References

Nishitani, N., Y. Hamaguchi, and T. Hori, Development of remote HF wave receiver in the backlobe direction of the SuperDARN Hokkaido East radar: Initial observations, Polar Sci., https://doi.org/10.1016/j.polar.2021.100669, 2021.

Autonomous detection of VLF triggered emissions using CNN

Yuki Detambo[1], Takahiro Watanabe[1], Mitsunori Ozaki[1] and Satoshi Yagitani[1]
[1]*Kanazawa University, Kanazawa, Japan*

VLF triggered emissions are electromagnetic wave emissions having frequency variations, which are excited from artificial radio waves with a constant frequency through energy transfer from space plasmas. It is believed to play an important role in controlling plasma energy through the wave-particle interactions. In this study, we developed an autonomous detection of VLF triggered emissions based on a Convolutional Neural Network (CNN) model. To mitigate the false detection of the triggered emissions caused by the noise effects in the wave observations data using a threshold detection, we used a CNN for the detection of the triggered emissions. We were able to reduce the false detection rate of the observation events by 39.4% in comparison with a threshold detection. For future work, we will study statistical analyses on the physical characteristics of the triggered emissions, such as frequency variation rate and wave intensity etc., to quantitatively clarify the features of nonlinear wave growth. In this presentation, we will present our CNN model and the evaluation results of the detection of the triggered emissions in detail.

OSp21

Next Generation DFMC SBAS broadcasted from QZSS in Ny-Ålesund

Toru Takahashi[1], Takanori Nishiyama[2] , Mitsunori Kitamura[1], Susumu Saito[1], Taishi Hashimoto[2] and Takeyasu Sakai[1, 3]
[1]*Electoronic Navigation Research Institute, National Institute of Maritime, Port and Aviation Technology, Tokyo, Japan*
[2]*National Institute of Polar Research, Tokyo, Japan*
[3]*Course of Maritime Technology and Logistics, Graduate School of Marine Science and Technology, Tokyo University of Marine Science and Technology, Tokyo, Japan*

Nowadays, aviation and maritime activities in the Arctic are growing with the decline in Arctic Sea ice (Miller and Ruiz, 2014). This decline in the Arctic Sea ice is expected to increase maritime activities regarding ocean resources and vessel traffic. Aviation activity is also expected to increase with the increase in maritime activities. A model study suggested that the Global Navigation Satellite System (GNSS), which operates with the augmentation system such as the Satellite-based augmentation systems (SBAS) and Advanced Receiver Autonomous Integrity Monitoring (ARAIM), is effective for the navigation of aviation and maritime in the Arctic because of poor infrastructures (Reid et al., 2016). However, the current L1 SBAS broadcasts augmentation messages from geostationary (GEO) satellites, which are not available practically in the polar region at a latitude of 72 degrees or higher. The Dual Frequency Multi Constellation Satellite Based Augmentation System (DFMC SBAS) has been standardization by the International Civil Aviation Organization (ICAO). Broadcasting augmentation messages from the Inclined Geosynchronous Orbit (IGSO) satellite is considered to be included in the future updates. The Electronic Navigation Research Institute (ENRI) developed the DFMC SBAS prototype based on the draft standards (Kitamura et al., 2018), and test messages are broadcasted from the Japanese Quasi-Zenith Satellite System (QZSS).

Takahashi et al. (2022) conducted an evaluation of the performance of DFMC SBAS broadcasted from QZSS in Oslo, Norway (10.72 deg. E, 59.94 deg. N) from 24 February 2021 to 17 March 2021. They successfully received the DFMC SBAS messages from QZSS, and GPS, Galileo, GLONASS, and BeiDou signals. They analyzed the errors in the position solutions as well as vertical and horizontal protection levels by using GPS L1/L5 and Galileo E1/E5a signals augmented by the DFMC SBAS. The positioning errors did not exceed the protection level, and the availability was 84.8% during this time interval. In this study, we concluded that the augmentation message could be used in the Arctic region, and suggested that the availability will be improved if three or more monitor stations are newly installed in the European region.

As a next step, we installed a GNSS receiver, a DFMC SBAS receiver, and a USRP in Ny-Ålesund, Norway (78.9°N, 11.9°E) on August 7, 2024. In this location, augmentation messages from GEO satellites are not practically received. The QZSS satellites rise to an elevation angle of ~20 degrees and are visible almost 24 hours a day. The ionosphere above Ny-Ålesund is frequently disturbed by geomagnetic activity, which may cause fluctuations in the GNSS carrier phase, known as phase scintillation. The objective of this study is to conduct a performance evaluation of the DFMC SBAS broadcast from the QZSS satellites and evaluate the impact of geomagnetic activity on the DFMC SBAS in the Arctic. The GNSS ranging signals were received by a JAVAD DELTA equipped with a reference clock input. A Stanford Research FS 725 generates a precise 10 MHz reference clock, which is input to the JAVAD DELTA. This reference clock allows us to derive phase scintillations associated with plasma density disturbances in the ionosphere. The CORE Chronosphere was used for receiving DFMC SBAS messages. The antenna used is a Tallysman Veraphase 6000, capable of receiving signals in the L1, L2, and L5 frequency bands. In this presentation, we will describe our project and its strategy, as well as present the initial results of the DFMC SBAS performance evaluation in Ny-Ålesund.

References

Miller, A. W., & Ruiz, G. M., Arctic shipping and marine invaders. Nature Climate Change, 4(6), 413–416. https://doi.org/10.1038/nclimate2244, 2014.

Reid, T., Walter, T., Blanch, J., & Enge, P. (2016). GNSS integrity in the arctic. NAVIGATION, 63(4), 469–492. https://doi.org/https://doi.org/10.1002/navi.169 , 2016.

T. Takahashi, S. Saito, M. Kitamura, T. Sakai, Performance of DFMC SBAS broadcasted from Japanese QZSS in Oslo, Norway, Proceedings of the 2022 International Technical Meeting of The Institute of Navigation, Long Beach, California, January 2022, pp. 401-406. https://doi.org/10.33012/2022.18239, 2022.

OSp22

Upper thermospheric orthohelium, He(2^3S) , variations associated with a moderate storm in February 2023: the NIRAS-2 observations at Longyearbyen (78.1◦N, 16.0◦E), Svalbard.

Takanori Nishiyama[1,2], Masato Kagitani[3], Tikemani Bag[1], Takuo T. Tsuda[4],
Yuki Iwasa[5], Yasunobu Ogawa[1,2], and Fred Sigernes[6]

[1]*National Institute of Polar Research*

[2]*Department of Polar Science, The Graduate University for Advanced Studies, SOKENDAI*

[3]*Planetary Plasma and Atmospheric Research Center, Graduate School of Science, Tohoku University*

[4]*Department of Computer and Network Engineering, University ofElectro-Communications*

[5]*National Metrology Institute of Japan, National Institute of Advanced Industrial Science and Technology*

[6]*University Centre in Svalbard*

This study presents a time variability of metastable orthohelium, He(2^3S) , in polar region associated with a geomagnetic storm for the first time. Continuous 17-nights dataset of He(2^3S) airglow brightness at 1083 nm was obtained from a short-wavelength infrared imaging spectrograph (NIRAS-2) at Longyearbyen, Svalbard (78.1◦N, 16.0◦E). The observed He(2^3S) airglow brightness clearly displayed responses to a geomagnetic storm in different time scales. The He(2^3S) airglow brightness has began to decrease sharply within an hour of sudden commencement of the storm, and it was gradually decreased over the next few days and then recovered slowly. It was nicely agreed to helium density variations at 500-km altitude calculated by MSIS. The depletion of He(2^3S) was mainly caused by enhanced Penning ionization due to upwelling N_2 from the lower atmosphere; this was consistent with decreased O/N_2 ratio in MSIS and TIMED/GUVI measurements, and electron density depletion in F region observed by EISCAT Svalbard Radar (ESR). Additionally, sudden increases in He(2^3S) airglow brightness were clearly found associated with intermittent electron precipitations observed by the ESR. Therefore, direct impact by precipitating electron injected from the space to the polar upper atmosphere can play significant roles in production of He(2^3S) . The NIRAS-2 measurements have successfully demonstrated that column density of He(2^3S) from the upper thermosphere to the exosphere was drastically changed by forcing both from the lower atmosphere and from the space. He(2^3S) measurements will definitely improve our understanding of thermosphere ionosphere coupling system and extend the coverage of space weather forecasting up to the exobase.